






**Sorkin parameter for type-I spontaneous parametric down-conversion biphotons and matter waves**

F. C. V. de Brito <sup>1,\*</sup>, C. H. S. Vieira <sup>1,†</sup>, I. G. da Paz <sup>2,‡</sup>, J. B. Araujo <sup>3,§</sup> and M. Sampaio <sup>1,||</sup>

<sup>1</sup>*CCNH, Universidade Federal do ABC, Santo André - SP 09210-580, Brazil*

<sup>2</sup>*Universidade Federal do Piauí, Departamento de Física, Teresina - PI 64049-550, Brazil*

<sup>3</sup>*Departamento de Física Matemática, Instituto de Física, Universidade de São Paulo, C.P. 66.318, São Paulo - SP 05315-970, Brazil*

 (Received 25 July 2020; revised 30 December 2020; accepted 2 March 2021; published 17 March 2021)

Type-I spontaneous parametric down-converted biphotons can be described approximately by a double-Gaussian wave function in configuration space. Using an effective propagator in the Fresnel approximation, the time evolution and transversal spreading of the two-particle biphoton wave function allow us to evaluate the Sorkin parameter  $\kappa$ , which results from nonclassical path contributions of the kink type and loops to double- and triple-slit interferometry. This simple unidimensional model for the evaluation of  $\kappa$  predicts that kinked nonclassical paths may lead to  $\kappa \approx 10^{-5}$  for degenerate biphotons. We show that such a model reproduces well the Sorkin parameter for matter waves found in more involved approaches in the literature. Moreover, we establish a hierarchy of approximations based on the shape of the nonclassical paths for matter waves and compare their size with leading relativistic corrections to the propagator.

DOI: [10.1103/PhysRevA.103.033707](https://doi.org/10.1103/PhysRevA.103.033707)

**I. INTRODUCTION**

For over 200 years, Young’s interference experiment has been crucial in probing nature’s wave-particle duality. Interference phenomena allowed us to set strong arguments in favor of the wave nature of light [1], helped us understand the crystalline structure of materials [2], and showed that even large molecules, such as  $C_{60}$ , can behave like waves [3,4] in benchtop experiments. Remarkably, interference has made it possible to verify the physical reality of the electromagnetic potentials [5,6], rule out the existence of a luminiferous aether [7], and detect gravitational waves at the Laser Interferometer Gravitational-Wave Observatory, in what is arguably the most precise scientific experiment in human history [8].

The most typical Young’s experiment setup consists of a source, an opaque surface with two slits, and a screen at which the signal is detected. The Born rule states that if a quantum object is represented by a wave function  $\psi(\vec{x}, t)$ , than the probability density of detecting it at position  $\vec{x}$  and time  $t$  is given by the absolute square of the wave function [9]. In this way, when the standard superposition principle is applied in a double-slit experiment, it has been common to consider that the wave function at the screen is a superposition of two amplitudes: one corresponding to the particle going through the upper slit and the other through the lower slit; these are usually called classical trajectories. However, we run into trouble as the full problem (propagation through two simultaneously open slits) is not equivalent to the sum of those

two possibilities (a single open slit at a time)—these configurations do not possess the same boundary conditions. Of course, the problem is well posed. The probability amplitude for a particle to be at a space-time point  $(\vec{x}_B, t_B)$  given that it started at  $(\vec{x}_A, t_A)$  is given by the Feynman path integral

$$\langle x_B | x_A \rangle = \int \mathcal{D}[x] e^{\frac{i}{\hbar} S[x]}, \tag{1}$$

where  $S[x]$  is the classical action, subjected to the constraints  $x(t_A) = \vec{x}_A$  and  $x(t_B) = \vec{x}_B$  [10]. For a potential representing a multislit barrier, this is an overwhelmingly difficult problem even if treated numerically [11]. This poses an interesting and fundamental question: Can we test the validity of Born’s rule and the superposition principle in multislit diffraction with light or matter waves? For this purpose, one needs to consider leading nonclassical (exotic or subleading) trajectories that contribute to (1) in a Young-type experiment. Yabuki [12] exploited the contributions from such nonclassical paths to the interference pattern in a double-slit experiment using both loops and kinks as shown in Fig. 1.

For massive particles, two- and three-dimensional models were implemented using a modified effective free particle propagator to account for the exotic paths. The effect of nonclassical trajectories on the experiment’s outcome is quantified by the Sorkin parameter  $\kappa$ , originally introduced in Ref. [13]. In a multislit experiment, if  $\psi_{A,B,C}$  represents the wave function at the detector for a particle emerging from slits  $A, B, C$ , the probability of detection at the screen is given by Born’s rule:

$$P_A = |\psi_A|^2, \quad P_{AB} = P_A + P_B + 2\text{Re}(\psi_A^* \psi_B),$$

$$P_{ABC} = P_{AB} + P_{BC} + P_{AC} - P_A - P_B - P_C. \tag{2}$$

Notice that for three or more slits, one always has a sum of terms denoting the interference of pairs of wave functions. A

\* [crislane.brito@ufabc.edu.br](mailto:crislane.brito@ufabc.edu.br)

† [vieira.carlos@ufabc.edu.br](mailto:vieira.carlos@ufabc.edu.br)

‡ [irismarpaz@ufpi.edu.br](mailto:irismarpaz@ufpi.edu.br)

§ [jbaraujo@if.usp.br](mailto:jbaraujo@if.usp.br)

|| [marcos.sampaio@ufabc.edu.br](mailto:marcos.sampaio@ufabc.edu.br)

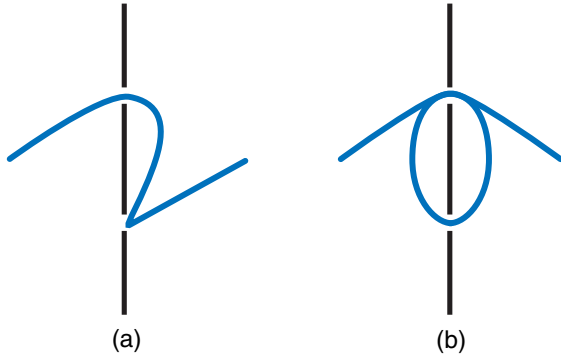


FIG. 1. Lowest-order single-particle nonclassical trajectories. (a) are referred to as kinks and (b) as loops.

possible contribution from higher order terms is measured by

$$\varepsilon = P_{ABC} - P_{AB} - P_{BC} - P_{AC} + P_A + P_B + P_C, \quad \kappa \equiv \varepsilon/I_{\max}, \quad (3)$$

in which the Sorkin parameter, here, has been normalized with respect to the intensity at the central maximum  $I_{\max}$  in the interference pattern as defined in Ref. [14].

In Ref. [15], the validity of Born's rule was verified through the experimental observation of exotic (looped) trajectories for the light by directly measuring their contribution to the formation of optical interference fringes in a triple slit. Such exotic paths were enhanced with electromagnetic fields in the vicinity of the slits. The authors have verified that nonclassical paths were related to the near-field component of the photon's wave function. Thus, by controlling the strength and spatial distributions of the near fields around the slits, they claimed that the probability of looped trajectories were increased, leading to  $\kappa \approx |0.25|$  for  $x$ -polarized heralded photons of wavelength 810 nm produced by degenerate down conversion in such a way that there was only one photon at a time in the experimental setup. The geometry involved a triple slit with height  $h = 100 \mu\text{m}$ , slit width  $w = 200 \text{ nm}$ , and interslit separation  $d = 4.6 \mu\text{m}$ . Conversely,  $\kappa$  is almost zero when no enhancement was performed. By measuring each term in Eqs. (3), U. Sinha *et al.* [16] performed a three-slit experiment using different photon sources such as an attenuated laser source down to  $\approx 200 \text{ fW}$  and heralded single photons produced via spontaneous parametric down conversion (SPDC) of wavelength 810 nm. The typical sizes in their triple-slit apparatus were  $h = 300 \mu\text{m}$ ,  $w = 30 \mu\text{m}$ , and  $d = 100 \mu\text{m}$ . They determined a bound on the accuracy of Born's rule, namely, that third-order interference was less than  $10^{-2}$  of the expected second-order contributions given by Born's rule. Moreover, semianalytic and numerical methods were used in estimates for the Sorkin factor  $\kappa$ . For instance, in Ref. [14], an energy space propagator was used for both photons and electrons,

$$K(\vec{r}_1, \vec{r}_2) = \frac{k}{2\pi i} \frac{e^{ik|\vec{r}_1 - \vec{r}_2|}}{|\vec{r}_1 - \vec{r}_2|}, \quad (4)$$

which satisfies the Helmholtz equation away from  $\vec{r}_1 = \vec{r}_2$  and the Fresnel-Huygens principle  $K(\vec{r}_1, \vec{r}_3) = \int d\vec{r}_2 K(\vec{r}_1, \vec{r}_2)K(\vec{r}_2, \vec{r}_3)$  for  $\vec{r}_2$  integrated over a plane between

$\vec{r}_1$  and  $\vec{r}_3$  perpendicular to  $\vec{r}_1 - \vec{r}_3$ . Such transitivity property is essential to write such a propagator in a path integral form [11]

$$K(\vec{r}_1, \vec{r}_2) = \int \mathcal{D}[\vec{x}(s)] \exp[ik \int ds],$$

where  $\mathcal{D}[\vec{x}(s)]$  is the functional integration over the paths  $\vec{x}(s)$  connecting  $\vec{r}_1$  and  $\vec{r}_2$ . Thus, nonclassical path contributions to  $\kappa$  are numerically estimated in a triple-slit setup in the far-field (Fraunhofer) regime. In the thin-slit approximation, for incident photons of wavelength  $\lambda = 810 \text{ nm}$ ,  $w = 30 \mu\text{m}$ , and  $d = 100 \mu\text{m}$ , distance between source and slits and slits and detector equal to 18 cm, they found  $\kappa \approx 10^{-6}$ , whereas for electrons of  $\lambda = 50 \text{ pm}$ ,  $w = 62 \text{ nm}$ ,  $d = 272 \text{ nm}$ , source-slit separation 30.5 cm and slit-screen distance 24 cm,  $\kappa$  was estimated as  $\approx 10^{-9}$ . Within their model, they were able to verify that keeping other experimental parameters fixed,  $\kappa$  increases with an increase in  $\lambda$ , arriving at  $\kappa \approx 10^{-3}$  for the microwave regime and macroscopic distances such as  $w = 1.2 \text{ m}$  and  $d = 4 \text{ m}$ . Later, an analytical description for the Sorkin parameter was derived and allowed for testing the role played by geometrical parameters on its determination [17]. In that work, the authors obtain good agreement with the results of Ref. [14] as well as with sophisticated and enduring numerical finite-difference time-domain (FDTD) solutions of Maxwell's equations for realistic models of three-slit devices presented in Ref. [18]. In their analytical description for  $\kappa$  using (3) and the propagator (4), successive approximations were possible assuming thin-slit and Fraunhofer limits (namely, source-slit and slit-screen distances much greater than any other length scale). Moreover, in the Fresnel regime where such approximations are not valid, a C++ code using Riemannian integration was used in Ref. [17]. They have tested their code for the same parameters used for the photons in Ref. [14] with a slit height  $h = 300 \mu\text{m}$ . Starting with a slit-screen separation of  $D = 20 \text{ cm}$  which yields  $|\kappa| \approx 6 \times 10^{-7}$ , the value of  $|\kappa|$  seems to increase as  $D$  diminishes, reaching a sudden peak at  $D \approx 1.3 \text{ cm}$  which the authors attribute to a breakdown of the paraxial approximation in the extreme near-field regime. Another interesting breakthrough from the experimental viewpoint was reported in Ref. [19]. Using a triple-slot experiment in the microwave domain, the authors obtained a nonzero  $\kappa$  using a pyramidal horn antenna as a source of electromagnetic waves of  $\lambda = 5 \text{ cm}$  which reached 10-cm-wide slots and interslot distance 13 cm. In addition, baffles were introduced inside the slits, allowing for studying a hierarchy of subleading paths contributing to  $\kappa$ .

Experiments testing the superposition principle to set bounds for the validity of Born's rule using massive particle multipath interferences were performed in Ref. [20]. Cotter *et al.* used a source of molecules with  $M = 515 \text{ amu}$  and Broglie wavelength  $\lambda_{dB} = 2.5 \leftrightarrow 5.0 \text{ pm}$ . The diffraction mask was composed by single, double, and triple slits of width  $w = 80 \text{ nm}$  with periodicities  $d = 100 \text{ nm}$  and  $d = 200 \text{ nm}$  for the double and  $d = 100 \text{ nm}$  for the triple slit. In their experiment, a different definition of  $\kappa$  was used, namely, the normalization in Eqs. (3) was taken with respect to the total number of molecules detected for a given Broglie wavelength leading to  $|\kappa| \leq 10^{-2}$ . Likewise, metastable

helium atoms were used in Ref. [21]. They have relied on a large number of counting statistics ( $1.7 \times 10^6$  counts in total) to obtain four diffraction patterns with a diffraction mask similar to Ref. [20] with  $w = 84.5$  nm,  $d = 136.5$  nm, and  $h = 1.6$  mm. The mask was placed at  $\approx 60$  mm from the collimation device and 800 mm from the detection screen. Therefore, with that experiment, a new bound to Born's rule using massive particle multipath diffraction was established at  $|\kappa| \leq 2.9 \times 10^{-5}$ .

A simplified analytical model to evaluate the Sorkin parameter for matter waves was constructed in Refs. [22,23,25]. The authors consider a physical setup in which the quantum effects manifest chiefly in the transversal direction, say  $\hat{x}$ , alongside the slit widths and perpendicular to the momentum  $\vec{p} = p_z \hat{z}$  of the particles emitted by the source. This turns out to be a good approximation in the limit where  $\Delta p_z \ll p_z$ , allowing for treating the motion in the  $z$  direction as classical since  $p_z$  is sharply defined [4]. The multislit interference pattern at the screen along the  $x$  direction is obtained analytically through explicit integration using Gaussian-shaped apertures. To assess the time spent by the particle during the interslit evolution of exotic paths, the authors exploit the momentum uncertainty in the  $x$  direction which is roughly  $\epsilon \equiv md/(\Delta p_x)$ . In Ref. [22], it was verified for electron waves that the Gouy phase difference  $|\delta\mu_G|$  is due to phases of nonclassical path contributions. Thus,  $|\delta\mu_G|$  serves as a signal and measure of nonclassical paths which led to  $\kappa \approx 10^{-8}$  in a triple-slit construction in accordance with Ref. [14]. Using the same unidimensional model, a double-slit setup using two-level atoms and QED cavities positioned at the slit apertures was constructed in Ref. [23]. The purpose was to account for the contribution of exotic trajectories only in the interference pattern via which-way information about the atoms. In this sense, in Ref. [24] it was shown that nonclassical paths yield different interference patterns using one and two which-way detectors in a double-slit experiment with light waves. This *gedanken* experiment was claimed to provide a new parameter (different from  $\kappa$ ) to test Born's rule, considering exotic paths as displayed in Fig. 1(a) and the propagator 4 in the Fraunhofer and stationary phase approximation. Finally, in another contribution [25] that employs the unidimensional model, a two-slit experiment was modeled with cold neutrons using the following parameters:  $m_n = 1.67 \times 10^{-27}$  kg,  $d = 125$   $\mu$ m,  $w = 7$   $\mu$ m, source-slit distance  $z_T = 5.0$  m, slit-screen distance  $z_r = 5.0$  m,  $\lambda_{dB} = 2$  nm, interslit propagation time  $\epsilon = 19.6$  ms, leading to  $\kappa \approx 10^{-5}$ . Their analysis also allows for studying the behavior of  $\kappa$  with  $z_r$  (Fresnel regime). Moreover, the authors showed that the Sorkin parameter can be related to the visibility and axial phases (such as the Gouy phase) and thus they could be used as alternative quantifiers for exotic paths.

In this contribution, we employ the one-dimensional model constructed in Refs. [22,23,25] to evaluate the Sorkin parameter. We address some questions related to the level of approximations involved in the analysis of kinked and looped nonclassical paths for both matter and light particles using double- and triple-slit constructions. The main advantage of this simplified model is that it is completely analytical and reproduces the order of magnitude of Sorkin parameters computed with more sophisticated approaches. Furthermore, we

show that our approach can be extended to the effective biphoton wave function in the configuration space which describes twin photons produced by type-I SPDC (SPDC-I) [26]. Because the signal of nonclassical paths in the interference pattern is a relatively tiny effect, we assess the contribution of relativistic effects in the interference pattern to compare with exotic path contributions. Simple analytical methods are useful as they provide hints for experimentalists to detect such small effects.

This paper is organized as follows. In Sec. II, we outline from first principles the approximations involved in the construction of biphoton wave functions as well as the entanglement measures and parameters encoded in a double Gaussian approximation. We also derive an effective propagator which describes the time evolution of the wave packets and interference in the transversal direction. Section III presents a consistency check of the framework in which it is verified that two entangled particles of wavelength  $\lambda$  can behave as a biphoton of wavelength  $\lambda/2$ . The Sorkin parameter  $\kappa$  in a double- and triple-slit setup is defined in Sec. IV, where we also compute the leading order contributions to  $\kappa$  for a biphoton produced via type-I SPDC. Moreover, within our framework, we compute the leading order contributions of nonclassical paths for matter waves (electron) and show that they are in agreement with more involved numerical and analytical methods in the literature. We finish that section by establishing a hierarchy of nonclassical paths (kinks and loops) that contribute to  $\kappa$  and compare their magnitude to relativistic corrections to the propagators. In Sec. V, we draw our final remarks and conclusions and we leave the bulky formulas to the Appendices.

## II. SPDC-I BIPHOTON WAVE FUNCTION

A first quantized theory of a photon is in principle not achievable because the photon is a massless relativistic quantum particle and thus is intrinsically described within (second quantized) quantum field theoretical formalism. Due to gauge symmetry, the appropriate degree of freedom is the electromagnetic potential  $A_\mu$ . This fact does not prevent us from (a) describing the low intensity limit of a double-slit experiment with light within wave mechanics, (b) defining an approximate position eigenstate for a photon, nor (c) investigating a quantum-mechanical description of optical beams [27]. One plausible approach from Oppenheimer [28] is based on an extension of the Weyl equation for massless neutrinos by replacing the Pauli vector with an angular momentum operator for spin-1 particles. A nice review can be found in Ref. [29]. The resulting six-component bispinors have positive and negative frequencies and can be interpreted as energy wave functions of photons and antiphotons, respectively. Moreover, a Lorentz invariant measure for the scalar product can be defined as well as an approximate position state. However, the propagator and time-dependent correlations within this approach is a tricky problem mainly due to the fact that photons are nonlocalizable. In Ref. [30], a modification in the Fourier transform to define the photon wave function was proposed. Whichever effective model one uses to describe a photon, it is important to take into account the process which generates it. In Ref. [31] was presented a wave function description

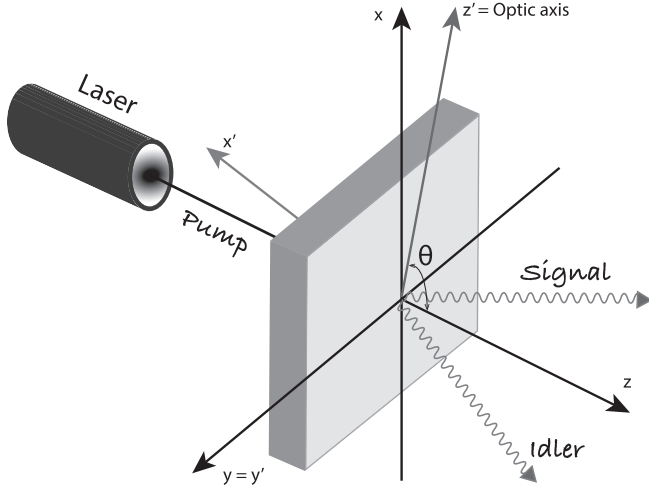


FIG. 2. Type-I SPDC process. An uniaxial crystal of optical axis  $z'$ . Ordinary rays have polarization in a direction perpendicular to the plane  $zz'$ . Extraordinary rays have polarization on the plane  $zz'$  and experiences a refractive index  $n_e(\theta)$  that depends on the angle  $\theta$  between the optical axis and the longitudinal direction  $z$  [26].

of a photon in Young’s double-slit experiment in which the photon source is a single excited atom (see also Ref. [32]). Moreover, in Ref. [33], a second quantized version of the Bialynicki-Birula-Sipe photon wave function [34] formalism was extended to include the interaction between photons and continuous (nonabsorptive) media. As an application, the quantum state of the twin photons generated by SPDC was derived. That being said, an effective wave-function treatment of photon states is possible and tools from Schroedinger wave mechanics may provide insights on various aspects of quantum light.

SPDC occurs when a nonlinear and usually birefringent crystal is hit by an incoming photon at (pump) frequency  $\omega_p$  which in turn is converted into two new outgoing photons of frequencies  $\omega_s$  (signal) and  $\omega_i$  (idler) with  $\omega_p = \omega_i + \omega_s$  and  $\vec{k}_p = \vec{k}_i + \vec{k}_s$ . The polarization properties of the photon pair define the resulting spatial distribution and serve to characterize the SPDC phenomenon. A type-I SPDC process happens when the polarization of the outgoing photons is parallel to each other and orthogonal to the polarization of the incoming photon. The spatial distribution of the emerging photons forms a cone that is aligned with the pump beam propagation with the apex at the crystal (Fig. 2). The state of a down-converted photon pair may be constructed based on some reasonable simplifying assumptions [26,35–37], such as that the crystal dimensions are large as compared to typical photon wavelengths, the crystal nonlinear susceptibility tensor is a slowly varying function of the frequencies, the pump field is a narrow band around  $\omega_p$ , and that its field amplitude does not vary significantly as it travels across the crystal. We can therefore write

$$|\Psi\rangle_{\text{SPDC}} \approx C_0|0_1, 0_2\rangle + C_1 \int_{\vec{k}_1, \vec{k}_2} \sqrt{\omega_1 \omega_2} \Phi(\vec{k}_1, \vec{k}_2) \times \hat{a}_{\vec{k}_1}^\dagger \hat{a}_{\vec{k}_2}^\dagger |0_1, 0_2\rangle, \quad (5)$$

where 1, 2 are signal/idler photon indices,  $C_{0,1}$  are normalization constants,  $\int_{\vec{k}_i} \equiv \int d^3\vec{k}_i / (2\pi)^3$  and

$$\Phi(\vec{k}_1, \vec{k}_2) = \mathcal{N} \delta(\omega_1 + \omega_2 - \omega_p) \delta^2(\vec{q}_1 + \vec{q}_2 - \vec{q}_p) \times \text{sinc}\left(\frac{\Delta k_z L_z}{2}\right) \tilde{E}(\vec{q}_1 + \vec{q}_2). \quad (6)$$

In the equation above,  $\mathcal{N}$  is a normalization constant,  $\Delta k_z \equiv k_{1z} + k_{2z} - k_{pz}$ ,  $\vec{q}_i$  are the momenta in the transversal direction, namely,  $\vec{k} = (\vec{k}^T, k_z^L) \equiv (\vec{q}, k_z \hat{z})$ , and  $L_z$  is the crystal thickness.

In addition, as in the Fresnel (paraxial) approximation  $|\vec{q}|^2 \ll |\vec{k}|^2$ , it is possible to express  $k_z$  in terms of the transverse components  $\vec{q}$  [26,36] to yield

$$\Phi(\vec{q}_i, \vec{q}_s) = \mathcal{N}_S \text{sinc}(b^2 |\vec{q}_i - \vec{q}_s|^2) e^{-|\vec{q}_i + \vec{q}_s|^2 / \sigma_\perp^2}. \quad (7)$$

In (7),  $b^2 \equiv \frac{L_z}{4k_{ep}}$ ,  $k_{ep} \equiv n_e(\theta)\omega_p/c$ ,  $\mathcal{N}_S$  is the normalization and we assumed that the transverse pump momentum profile is Gaussian  $\tilde{E}(\vec{q}_i + \vec{q}_s) = \tilde{\mathcal{N}} e^{-|\vec{q}_i + \vec{q}_s|^2 / \sigma_\perp^2}$ , which is nothing but a statement of the uncertainty in transverse momentum conservation. The  $\vec{q}_i - \vec{q}_s$  argument in the sinc function expresses energy and (longitudinal) momentum conservation. Notice that  $\Phi(\vec{q}_i, \vec{q}_s)$  is not separable into factors depending on  $\vec{q}_i$  and  $\vec{q}_s$  and therefore it is entangled (not factorable).

In Ref. [38], it was shown that the degree of entanglement is governed by the product  $\sigma_\perp b$ . High entanglement is achieved when either  $\sigma_\perp b \gg 1$  or  $\sigma_\perp b \ll 1$ , the minimum occurring for  $\sigma_\perp b \approx 1$ . Moreover, the sinc representation of the biphoton wave function is more entangled than its Gaussian approximation, which we shall discuss below, for the same values of  $\sigma_\perp b$ . Moreover, this biphoton wave function is approximately separable [35] (subject to the paraxial approximation) into a product of functions, one dependent on only  $x$  coordinates and the other dependent on only  $y$  coordinates). That is because for small values of  $x$  and  $y$ ,  $\text{sinc}(x+y) \sim \text{sinc}(x)\text{sinc}(y)$ . In the paraxial approximation, the transverse momenta are much smaller than the pump momentum, and so the arguments of the sinc functions are very small ( $\approx 10^{-3}$ ) [35]. Thus, writing the  $y$  component  $q_{iy}, q_{sy}$  simply as  $q_i, q_s$  yields

$$\Phi_S(q_i, q_s) = \tilde{\mathcal{N}}_S \text{sinc}(b^2 (q_i - q_s)^2) e^{-(q_i + q_s)^2 / \sigma_\perp^2}. \quad (8)$$

To study the spatial transversal correlations of the biphotons, we need to Fourier transform the wave function into coordinate space. Following Refs. [35,36,38–42], the sinc function may be approximated by a Gaussian

$$\Phi_G(q_i, q_s) = \tilde{\mathcal{N}}_G e^{-b^2 (q_i - q_s)^2} e^{-(q_i + q_s)^2 / \sigma_\perp^2}, \quad (9)$$

whose Fourier transform is

$$\Psi_G(y_-, y_+) = \frac{1}{\sqrt{2\pi\sigma_-\sigma_+}} e^{-\frac{y_-^2}{4\sigma_-^2}} e^{-\frac{y_+^2}{4\sigma_+^2}}, \quad (10)$$

where  $\sigma_- \equiv b/\sqrt{2}$ ,  $\sigma_+ \equiv \sqrt{2}\sigma_\perp$  and  $y_\pm \equiv \frac{(y_i \pm y_s)}{\sqrt{2}}$ . Also, we have normalized  $\Psi_G$  so  $\iint dy_- dy_+ |\Psi_G|^2 = 1$ . We shall adopt the double-Gaussian approximation for simplicity as it makes both transverse position and momentum statistics easy to calculate besides fitting well experimental data [43]. Moreover, as we shall see, the double-Gaussian wave function is easy to

propagate in time within the paraxial regime (the same regime used in the approximations of our biphoton state).

Consistent with the approximations that led to the down-converted biphoton wave function, under the conditions of validity of the Fresnel approximation, the diffraction and interference of a wave traveling in the  $z$  direction can be described in terms of its spreading in time of the wave-packet transversal  $(x, y)$  section [44]. For Broglie waves of massive particles, the wave-packet spreading is due to the dispersion relation  $\omega_k = \hbar k^2/(2m)$  and the free evolution is given by the Fourier transform

$$\psi(\vec{r}, t) = \int d^3k e^{i(\vec{k}\vec{r} - i\omega_k t)} \tilde{\psi}(\vec{k}, 0), \quad (11)$$

where  $\tilde{\psi}(\vec{k}, 0)$  is the Fourier transform of the initial condition. As for a biphoton wave traveling in the  $z$  direction, due to the fact that the sinc function factorizes in the transversal  $(x, y)$  directions for typical experimental parameters, we may disregard the  $x$  direction. In the case of a multislit diffraction, we could consider such waves impinging on a screen with slits along the  $x$  axis and study the spreading along the  $y$  axis. Thus, assuming symmetry along the  $x$  axis, we may disregard the  $x$  coordinate and write [44]

$$\Psi(y, z, t) = \psi(y, z) e^{-i\omega_0 t}, \quad (12)$$

in which  $\psi$  satisfies the Helmholtz equation  $\Delta\psi = -k_0^2\psi$  and  $\omega_0 = ck_0$ . Taking the one-dimensional Fourier transform,

$$\psi(y, z) = \frac{1}{\sqrt{2\pi}} \int \tilde{\psi}(k_y, z) e^{ik_y y} dk_y, \quad (13)$$

and using that  $\psi(y, z)$  satisfies the Helmholtz equation, we get, for progressive waves in the  $z$  direction,

$$\tilde{\psi}(k_y, z) = \tilde{\psi}(k_y, 0) e^{i\sqrt{k_0^2 - k_y^2} z}, \quad (14)$$

which, in the Fresnel approximation  $\sqrt{k_0^2 - k_y^2} \approx k_0 - k_y^2/(2k_0)$ , gives [44]

$$\psi(y, z) = e^{ik_0 z} \frac{k_0}{\sqrt{2\pi i z}} \int e^{i\frac{k_0}{2z}(y-y')^2} \psi(y', 0). \quad (15)$$

By identifying  $\psi(y, t=0) \equiv \psi(y, z=0)$ , we have  $|\psi(y, t)|^2 \equiv |\psi(y, z)|^2$  provided  $z = ct$ . Therefore, we arrive at the nonrelativisticlike propagator,

$$G(y, t; y', t') = \sqrt{\frac{\tilde{m}}{2\pi i \hbar (t - t')}} e^{i\frac{\tilde{m}(y-y')^2}{2\hbar(t-t')}}, \quad (16)$$

where  $\tilde{m} \equiv \frac{k_0 \hbar}{c}$  and we have dropped out a global phase factor  $e^{-i\frac{\tilde{m}c^2}{\hbar}(t-t')}$  which is immaterial. The propagator (16) was used in Ref. [41] in a double-slit experiment to demonstrate that a degenerate biphoton of wavelength  $\lambda$  produced via SPDC can behave as a single quanton of wavelength  $\frac{\lambda}{2}$  as seen in Ref. [39]. It was also employed in Ref. [26] to study a continuous-variable Bell violation for type I-SPDC biphotons. Finally, we write the free propagation of a biphoton SPDC wave function as

$$\begin{aligned} \Psi(y_i, y_s, t) &= \iint dy'_i dy'_s G(y_i, t; y'_i, 0) G(y_s, t; y'_s, 0) \\ &\times \Psi(y'_i, y'_s, 0). \end{aligned} \quad (17)$$

To make contact with the notation in the literature, let us redefine the biphoton coordinates such that

$$y_i \equiv x_1, \quad y_s \equiv x_2, \quad \sigma_- \equiv \sigma/\sqrt{2}, \quad \text{and} \quad \sigma_+ \equiv \Omega/\sqrt{2},$$

and therefore

$$\psi_0(x_1, x_2) = \frac{1}{\sqrt{\pi\sigma\Omega}} e^{-\frac{(x_1-x_2)^2}{4\sigma^2}} e^{-\frac{(x_1+x_2)^2}{4\Omega^2}}, \quad (18)$$

as well as new relative coordinates  $r = (x_1 + x_2)/2$  and  $q = (x_1 - x_2)/2$ , so

$$\psi_0(r, q) = \frac{1}{\sqrt{\pi\sigma\Omega}} e^{-\frac{q^2}{\sigma^2}} e^{-\frac{r^2}{\Omega^2}}. \quad (19)$$

Accordingly, after a time  $t$ , the evolved state in the  $\{r, q\}$  variables becomes, using (17)

$$\psi(r, q, t) = C \exp\left[\frac{-q^2}{\sigma^2 + \frac{i\lambda ct}{2\pi}}\right] \exp\left[\frac{-r^2}{\Omega^2 + \frac{i\lambda ct}{2\pi}}\right], \quad (20)$$

in which

$$C = \frac{1}{\sqrt{\pi\left[\sigma + i\left(\frac{\lambda ct}{2\pi}\right)\frac{1}{\sigma}\right]\left[\Omega + i\left(\frac{\lambda ct}{2\pi}\right)\frac{1}{\Omega}\right]}}. \quad (21)$$

To characterize the entanglement of the transverse canonical coordinates  $x_i$  and  $p_i$  for the biphotons, we follow Refs. [45–47]. The degree of entanglement can be quantified in the double Gaussian approximation in terms of the negativity of the partially transposed density matrix. The Duan criterion [48] is a sufficient criterion for nonseparability for a pair of EPR-type wave functions for continuous variables. For the wave function (20), it yields that the system is separable if  $\sigma = \Omega$ . Also, the Peres-Horodecki criterion [49] states that a Gaussian state is separable if and only if the minimum value of the symplectic spectrum of the partial transpose of the covariance matrix is greater than  $1/2$ , which leads to a measure of the entanglement  $E$  of the Gaussian state (20)

$$E = \log_{10} \left( \frac{\Omega}{\sigma} \right) \equiv E_{\mathcal{N}}, \quad (22)$$

that coincides with the expression for the logarithmic negativity  $E_{\mathcal{N}}$  [45] that establishes that the greater  $\Omega/\sigma$ , the larger the negativity and hence the larger the entanglement. Another useful quantity is the degree of spatial correlation (Pearson  $r$  value),

$$\rho_x = \frac{\langle x_1 x_2 \rangle - \langle x_1 \rangle \langle x_2 \rangle}{\sigma_{x_1} \sigma_{x_2}}, \quad (23)$$

which ranges from  $-1$  to  $+1$ , where  $\sigma_{x_{1,2}}$  is the standard deviation of  $x_{1,2}$ .  $\rho_x$  is zero if the two photons are uncorrelated, and  $\rho_x \rightarrow +1$  if they are spatially closely correlated (bunched) and  $\rho_x \rightarrow -1$  if they are spatially closely anticorrelated (antibunched). For the biphoton state described in (20), we get

$$\rho_x(t) = \frac{(\Omega^2 - \sigma^2) \left[ 1 - \left( \frac{\lambda ct}{2\pi\sigma\Omega} \right)^2 \right]}{(\Omega^2 + \sigma^2) \left[ 1 + \left( \frac{\lambda ct}{2\pi\sigma\Omega} \right)^2 \right]}. \quad (24)$$

Accordingly, it is possible to write the degree of spatial correlation  $\rho(t)$  as a function of the logarithmic negativity  $E_{\mathcal{N}}$  and time  $t$ —a few plots of  $\rho(E_{\mathcal{N}}, t)$  are shown in Fig. 3.

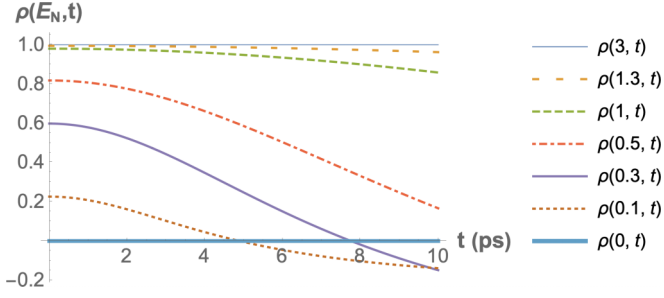


FIG. 3. Behavior of the degree of spatial correlation as a function of  $t$  (in picoseconds) for different values of logarithmic negativity  $E_N$ . One observes that for  $E_N \sim 3$ , the initial value of  $\rho(t)$  saturates at 1 and barely decreases for  $t = 4$  ps, which is the typical time it takes for the photons to reach the slits. For lower values of  $E_N$ , the decrease can be appreciable. We have used  $\sigma = 11.4 \times 10^{-3}$  mm,  $c = 0.3$  mm/ps, and  $\lambda = 7.02 \times 10^{-4}$  mm.

Transverse spatial correlations of biphotons produced via SPDC in the double Gaussian approximation were studied in Ref. [35]. At the sinc level, spatial correlations of biphotons were seen to encompass Bell nonlocality in Ref. [26]. In Ref. [41], a double Gaussian approximation was used to show an experimental verification [39,50] that two entangled photons of wavelength  $\lambda$  can behave like a single quantum of wavelength  $\lambda/2$ . Position-momentum Bell nonlocality via a Clauser-Horne-Shimony-Holt inequality violation using entangled biphotons has also been verified experimentally in Ref. [51]. The entanglement of degenerate type-I SPDC biphotons was studied using a spectral wave function beyond double Gaussian approximation in Ref. [52].

Biphoton double-slit interference has been studied both theoretically and experimentally in a series of articles: In Ref. [53], it was reported a nonlocal interference between SPDC biphotons measured in coincidence after passing through double slits. Similarly, the interference pattern of two indistinguishable photons sent to well-defined slits at an identical time was analyzed in Ref. [54]. Their data were in accordance with predictions based on standard quantum mechanics and in contrast with the deterministic Broglie-Bohm model. The role of mode functions and which-slit information in interference patterns of biphotons was experimentally assessed in Ref. [55]. Moreover, Young's double-slit interference with two-color biphotons was performed in Ref. [56], shedding further light on the interplay between interference and which-path information as a result of the nonlocal nature of two-photon entanglement.

### III. BIPHOTON INTERFERENCE IN A DOUBLE SLIT

Considering only classical trajectories the biphoton state at the screen, after passing through a double slit, can be written under the assumptions that led to (16) as

$$\begin{aligned} \psi(x_1, x_2, T + \tau) = & \int_X G(x_1, T + \tau; x'_1, T) \\ & \times G(x_2, T + \tau; x'_2, T) F_{u,d}(x'_1) F_{u,d}(x'_2) \\ & \times G(x'_1, T; x'_1, 0) G(x'_2, T; x'_2, 0) \psi_0(x'_1, x'_2), \end{aligned} \quad (25)$$

where the integrations from  $-\infty$  to  $+\infty$  are taken over  $\{X\} = \{x'_1, x'_2, x''_1, x''_2\}$ . The functions  $F$  represent the Gaussian-shaped windows [10], which crop the wave function at the slits, and  $T(\tau)$  is the time interval between source and slits (slits and screen). The window functions  $F_{u,d}(x'_1)F_{u,d}(x'_2)$  read

$$F_u(x_i) \equiv e^{-\frac{(x_i-d/2)^2}{2\beta^2}} \quad \text{and} \quad F_d(x_i) \equiv e^{-\frac{(x_i+d/2)^2}{2\beta^2}}, \quad (26)$$

where  $i = 1, 2$ ,  $u(d)$  stands for upper(lower)-slit,  $d$  is the interslit center-to-center distance and  $\beta$  the slit width. The integrals in Eq. (25) can be analytically computed to yield four amplitudes,

$$\psi_i = A_i \exp[C_i(r, q) + i\alpha_i(r, q)], \quad (27)$$

with  $C_i(r, q)$  and  $\alpha_i(r, q) \in \mathbb{R}$  and  $i = \{uu, dd, ud, du\}$  denote each of the biphoton possible paths through the upper or lower slit. The coefficients  $C_i$  and  $\alpha_i$  have the general forms

$$\begin{aligned} C_i(r, q) &= c_1 r^2 + c_2 q^2 + c_3 r + c_4 q + c_5, \\ \alpha_i(r, q) &= a_1 r^2 + a_2 q^2 + a_3 r + a_4 q + a_5, \end{aligned} \quad (28)$$

whose coefficients  $c_i$  and  $a_i$  are listed in Appendix A. The intensity at the screen is given by Born's rule,

$$I(x_1, x_2) = |\psi_{uu} + \psi_{ud} + \psi_{du} + \psi_{dd}|^2 = I(x_2, x_1), \quad (29)$$

as we have considered biphotons such that  $\lambda_1 = \lambda_2$  (degenerate case).

At this point, it is worthwhile to test our framework by verifying that the diffraction of a wave packet of two entangled photons, each of which of wavelength  $\lambda$  can display an interference pattern of a single quantum of wavelength  $\lambda/2$  [39,41]. The values of  $\Omega$  and  $\sigma$  are determined by the experiment. Typically,  $\sigma = \sqrt{L_z \lambda_p / (6\pi)} \approx 0.01$  mm [35,51]. Choosing  $E_N = 2$  (and thus high spatial correlation, see Fig. 3). For detection in coincidence  $x_1 = x_2 = x$  (or, equivalently,  $r = x$  and  $q = 0$ ), we get the solid blue line in Fig. 4. To verify whether a photon of the pair behave as a single particle, we may place one detector at the center of the slits ( $x_2 = 0$ ) and let the other sweep the screen to obtain the intensity depicted by the dotted line in Fig. 4. It is clear that the intensity for both photons detected at the same point oscillate with half the wavelength as compared with the single photon interference. This is in agreement with Ref. [50] in the sense that  $N$  particles of wavelength  $\lambda$  can behave like a single particle, or quantum, of wavelength  $\lambda/N$  in an interference experiment. For entangled biphotons, this has been verified in Ref. [36]. Moreover, in Ref. [41], it was argued that this effect can be verified in a nonlocal fashion as well. In our case, the high degree of spatial correlation at the slits ( $T \approx 4$  ps) turns the amplitudes  $\psi_{ud,du}$  highly suppressed, namely, the wave functions  $\psi_{ud,du}$  can be removed from the total intensity Eq. (29) with negligible effect (the fractional difference is of order  $\sim 10^{-15}$ ), which indicates the photons are likely to go through the same slit. A similar analysis was performed in Ref. [41], considering sharp slits and ignoring the middle terms in (29) for high spatial correlation.

### IV. SORKIN PARAMETER

Let us evaluate the Sorkin parameter due to the biphoton's nonclassical trajectories in double- and triple-slit setups. The

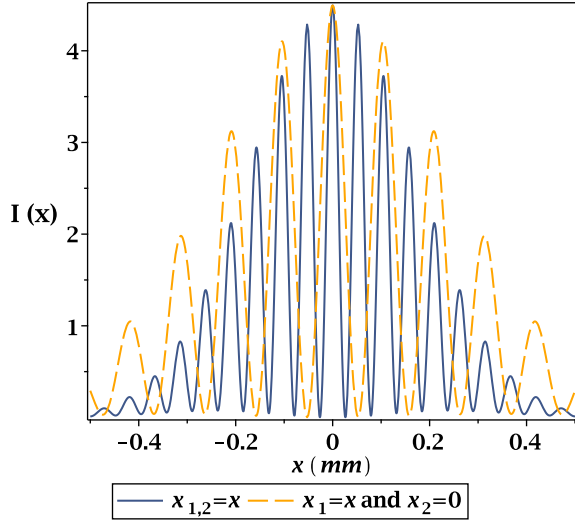


FIG. 4. Two photons of wavelength  $\lambda$  behaving as a single photon of wavelength  $\lambda/2$ . We used the set of parameters  $\lambda = 7.02 \times 10^{-4}$  mm,  $E_{\mathcal{N}} = 2$ ,  $\sigma = 11.4 \times 10^{-3}$  mm,  $\Omega = 10^{E_{\mathcal{N}}} \sigma$ ,  $\beta = 5 \times 10^{-3}$  mm,  $d = 0.1$  mm,  $c = 0.3$  mm/ps,  $t = 4$  ps, and  $\tau = 50$  ps. These parameter values do not differ considerably from the ones used in Ref. [54].

Sorkin parameter can be defined as

$$\kappa = \frac{I_{\text{total}} - I_c}{I_{\text{total}}(0)}. \quad (30)$$

For a single-particle triple-slit setup, according to Born's rule, the probability of detection at the screen is given by

$$I_{\text{total}} = I_{ABC} = |\psi_A + \psi_B + \psi_C + \psi_{\text{nc}}|^2, \quad (31)$$

where  $I_c = |\psi_A + \psi_B + \psi_C|^2$ ,  $\psi_i$  is for the wave function at the screen when a particle passes through slit  $i$ , and  $\psi_{\text{nc}}$  corresponds to any exotic, nonclassical trajectories.

For a biphoton double-slit setup, the total intensity is

$$I_{\text{total}} = |\psi_{uu} + \psi_{ud} + \psi_{du} + \psi_{dd} + \psi_{\text{nc}}|^2, \quad (32)$$

while the classical contribution reads

$$I_c = |\psi_{uu} + \psi_{ud} + \psi_{du} + \psi_{dd}|^2. \quad (33)$$

Next we describe the nonclassical trajectories and rank them according to their contribution to the Sorkin parameter.

#### A. Sorkin parameter for the biphoton: Double slit

In a two-slit interference experiment, we can have two types of nonclassical trajectories, involving either kinks or loops around the slits as in Fig. 1. For a two-particle wave function, one may include several possibilities, namely, one particle performing a nonclassical trajectory, while the other does a classical one, or both particles performing nonclassical paths. For the propagation between the slits, we employ the propagator

$$G_\epsilon(x_i, t + \epsilon; x_0, t) = \sqrt{\frac{1}{i\lambda c \epsilon}} \exp\left[\frac{-\pi(x_i - x_0)^2}{i\lambda c \epsilon}\right]. \quad (34)$$

An estimate for the interslit transit time  $\epsilon$  is given by  $\epsilon = d/\Delta v_x$ , where  $\Delta v_x = \Delta p_x/\tilde{m}$ ,  $\tilde{m} = k/\hbar c$  [26]) and

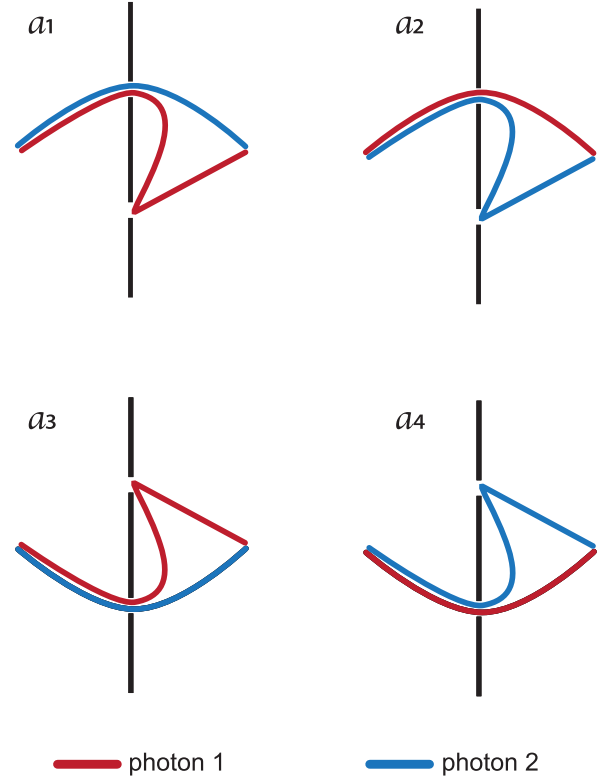


FIG. 5. The four contributions due to single-particle kink trajectories, when both photons go first through the same slit. These drawings represent same-position coincidence detection.

$\Delta p_x = \sqrt{\langle p_x^2 \rangle - \langle p_x \rangle^2}$  is the momentum uncertainty orthogonal to the propagation direction [22,23,25]. In the averages  $\langle p_x^2 \rangle$  and  $\langle p_x \rangle^2$ , we use the normalized wave function, including only classical trajectories, after the Gaussian-slit cropping. The simplest leading order contributions to the Sorkin parameter arise when one photon executes a kink and the other takes a classical trajectory, such as depicted in Figs. 5 and 6. Loop contributions are less relevant by several orders of magnitude (as one particle goes three times through the slits), and so are the ones in which both particles perform nonclassical trajectories.

The amplitude corresponding to photon 1 performing a kink (source  $\rightarrow$  upper slit  $\rightarrow$  lower slit  $\rightarrow$  screen) while photon 2 takes a classical trajectory (source  $\rightarrow$  upper slit  $\rightarrow$  screen), as depicted in Fig. 5( $a_1$ ), is obtained as

$$\begin{aligned} \psi_{\text{nc}(a_1)} = & \int G(x_1, T + \epsilon + \tau; x_1'', T + \epsilon) F_d(x_1''') \\ & \times G_\epsilon(x_1''', T + \epsilon; x_1', T) F_u(x_1') G(x_2, T + \tau; x_2', T) \\ & \times F_u(x_2') G(x_1'', T; x_1', 0) G(x_2'', T; x_2', 0) \psi_0(x_1', x_2'), \end{aligned} \quad (35)$$

where the integral is over all primed variables  $\{x_1', x_2', x_1'', x_2'', x_1'''\}$ . Other possible nonclassical paths for photons passing through the same slit are depicted in Fig. 5. They add up to

$$\Psi_{\text{nc}(a)} = \psi_{\text{nc}(a_1)} + \psi_{\text{nc}(a_2)} + \psi_{\text{nc}(a_3)} + \psi_{\text{nc}(a_4)}, \quad (36)$$

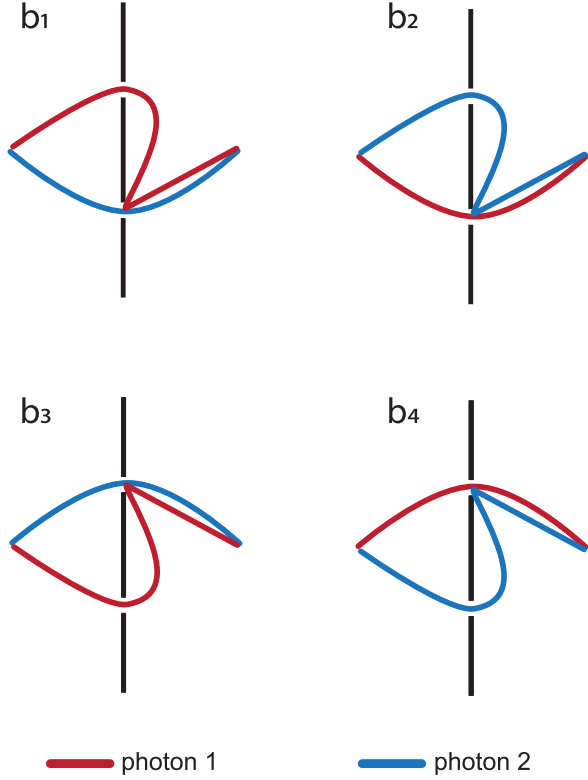


FIG. 6. The four contributions due to single-particle kink trajectories, when the photons go first through different slits. These drawings represent same-position coincidence detection.

whereas in Fig. 6, the amplitudes for photons passing through different slits result in

$$\Psi_{nc(b)} = \Psi_{nc(b_1)} + \Psi_{nc(b_2)} + \Psi_{nc(b_3)} + \Psi_{nc(b_4)}. \quad (37)$$

The weight of the contribution from the sets  $a$  and  $b$  is ruled by the degree of initial spatial correlation which, for the parameters specified in Fig. 3, is governed by  $E_N$  or ultimately by the ratio  $\Omega/\sigma$ . A lengthy but straightforward calculation for the analytical expressions of the contributions  $\Psi_{nc(a_i)}$  and  $\Psi_{nc(b_i)}$ ,  $i = \{1, 2, 3, 4\}$ , can be easily computed using MAPLE [57]:

$$\begin{aligned} \Psi_{nc(a_i, b_i)}(x_1, x_2) \\ = A_{nc(a_i, b_i)} \exp[C_{nc(a_i, b_i)}(x_1, x_2) + i \alpha_{nc(a_i)}(x_1, x_2)], \end{aligned} \quad (38)$$

where the coefficients  $C_{nc(a_i, b_i)}(x_1, x_2)$  and  $\alpha_{nc(a_i, b_i)}(x_1, x_2)$ , omitting the  $i$  index, have the general form

$$\begin{aligned} C_{nc(a, b)} &\equiv \bar{c}_1 x_1^2 + \bar{c}_2 x_2^2 + \bar{c}_3 x_1 x_2 + \bar{c}_4 x_1 + \bar{c}_5 x_2 + \bar{c}_6, \\ \alpha_{nc(a, b)} &\equiv \bar{a}_1 x_1^2 + \bar{a}_2 x_2^2 + \bar{a}_3 x_1 x_2 + \bar{a}_4 x_1 + \bar{a}_5 x_2 + \bar{a}_6, \end{aligned} \quad (39)$$

whose explicit expressions are found in Appendix B. We shall vary the logarithmic negativity  $E_N$ , which is related to  $\rho_x(t)$ , to evaluate the Sorkin parameter  $\kappa_{nc(a, b)}$  due to the contributions given by  $\Psi_{nc(a, b)}$  that can be written as

$$\kappa_{nc(a, b)} = \frac{I_{nc(a, b)} - I_c}{I_{nc(a, b)}(0, 0)}, \quad (40)$$

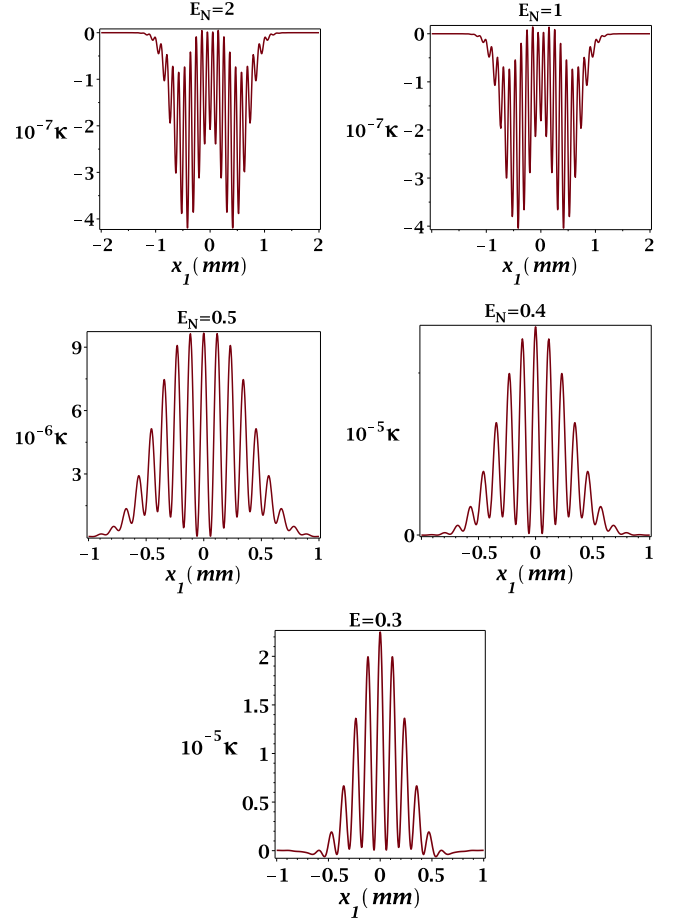


FIG. 7. Sorkin parameter  $\kappa_{nc-a}$  for different values of logarithmic negativity  $E_N$ . We used the set of parameters:  $T = 4$  ps,  $\tau = 50$  ps,  $\sigma = 11.4 \mu\text{m}$ ,  $\Omega = \sigma \times 10^{E_N}$ ,  $\lambda = 702$  nm,  $d = 100 \mu\text{m}$ ,  $\beta = 5 \mu\text{m}$ . In these plots, we have set  $x_2 = 0$  and swept over  $x_1$ . Observe that for  $E_N$  between 0.3 and 0.4 the Sorkin parameter increases about two orders of magnitude if compared to  $E_N \approx 1$ . The  $x_1$  coordinates are plotted in millimeters.

where

$$I_{nc(a, b)}(x_1, x_2) = |\Psi_{uu} + \Psi_{ud} + \Psi_{du} + \Psi_{dd} + \Psi_{nc(a, b)}|^2. \quad (41)$$

The intensity in Eq. (41) depends on  $x_1$  and  $x_2$ , which means that the Sorkin parameter will depend on the measurement procedure. The coincidence measurements involving nonclassical propagations takes a time interval  $\epsilon$  from slit to slit  $\sim 1$  ps. The time resolution of current counters is of the order of  $10^2$  ps [58], so the coincidence measurements are still inside the detectors' resolution. Our numerical analysis has shown that the Sorkin parameter for coincidence measurements such that  $x_1 = x_2$  detection does not differ considerably from, say,  $x_2 = 0$  and  $x_1 = x$  on the screen. Therefore, we will adopt the latter strategy. A few plots of  $\kappa_{nc(a)}$  for different  $E_N$  values can be found in Fig. 7. The Sorkin parameter is a function of both  $x_1$  and  $x_2$ , and we chose  $x_1 = x_2$  in the plots of Fig. 7. We remark that, in view of Eq. (30), the Sorkin parameter assumes positive and negative values in the  $x_1 - x_2$  plane, since its integral over it should be zero for normalized intensities.



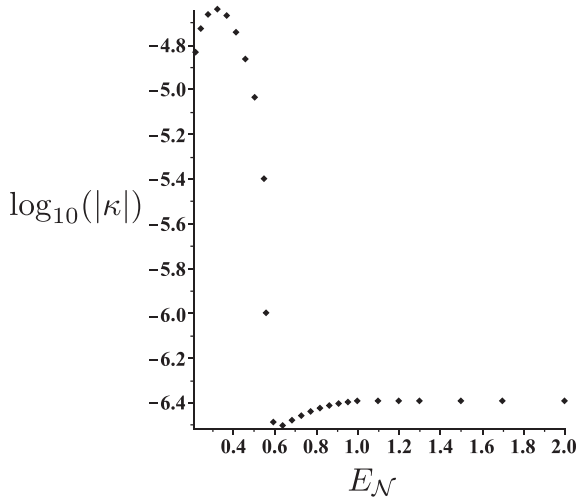


FIG. 8. Double slit: The behavior of the maximum value of the Sorkin parameter as a function of  $E_{\mathcal{N}}$  which shows that it has a maximum value  $\kappa \approx 10^{-5}$  for  $0.3 \lesssim E_{\mathcal{N}} \lesssim 0.4$  before stabilizing at  $10^{-7}$  for  $E_{\mathcal{N}} > 1$ .

The Sorkin parameters shown in Fig. 7 have values that are about one order of magnitude lower than the ones found in Ref. [17] (in which a three-slit setup for single photons was used) in the range  $E_{\mathcal{N}} \gtrsim 1$ . Remarkably, in the range  $E_{\mathcal{N}} = [0.2, 2]$ , the Sorkin parameter increases by about two orders of magnitude for  $0.3 \lesssim E_{\mathcal{N}} \lesssim 0.4$  ( $\kappa \approx 10^{-5}$ ), in comparison to  $E_{\mathcal{N}} \gtrsim 1$ . Qualitatively, large values of  $E_{\mathcal{N}} \gtrsim 1$  do not mean a larger Sorkin parameter, since photons are unlikely to separate in a nonclassical trajectory during the interslit transit time due to their spatial correlation. There is, however, an optimal region  $0.3 \lesssim E_{\mathcal{N}} \lesssim 0.4$  that yields an increase to the Sorkin parameter because the nonclassical trajectories are not as suppressed as for large negativities  $E_{\mathcal{N}}$ . On the other hand, for  $E_{\mathcal{N}} \lesssim 0.2$ , we observed that the Sorkin parameter becomes negligible since the biphotons are unlikely to diffract through the same slit. Figure 8 shows the plot of  $\log_{10}(|\kappa|)$  against  $E_{\mathcal{N}}$  for the double slit parameters specified in Fig. 7.

Moreover, the contributions from the trajectories in Fig. 6 to the Sorkin parameter  $\kappa_{nc(b)}$  are negligible compared to  $\kappa_{nc(a)}$ . This is a consequence of the short transit time between the SPDC crystal and the slits, which favors biphotons going first through the same slit. Accordingly, by increasing the transit time between source and slits, the contributions of types  $\kappa_{nc(a)}$  and  $\kappa_{nc(b)}$  become comparable. Numerical evaluations have shown that, by using the same set of parameters from Fig. 7,  $E_{\mathcal{N}} = \{2, 1, 0.5, 0.4, 0.3\}$  one obtains, respectively,  $\kappa_{nc(b)} \sim \{10^{-22}, 10^{-22}, 10^{-17}, 10^{-15}, 10^{-13}\}$ .

The spatial correlations as given by the Pearson's value at the slits,  $\rho_x(T)$ , do not determine by themselves the value of the Sorkin parameter. The logarithmic negativity  $E_{\mathcal{N}}(\sigma, \Omega)$ , which is constant up to the grating, is related to  $\rho_x(t)$  through Eq. (24). For the double-slit setup and the exotic paths of the configuration  $\kappa_{nc(a)}$ , we can study how the Sorkin parameter varies with  $\rho_x(T)$ ,  $T$  being the typical flight time from the source to the grating. In Fig. 9, we plot the (logarithm of)  $\kappa$  as a function of the Pearson's value after choosing  $E_{\mathcal{N}} = 0.4$ .

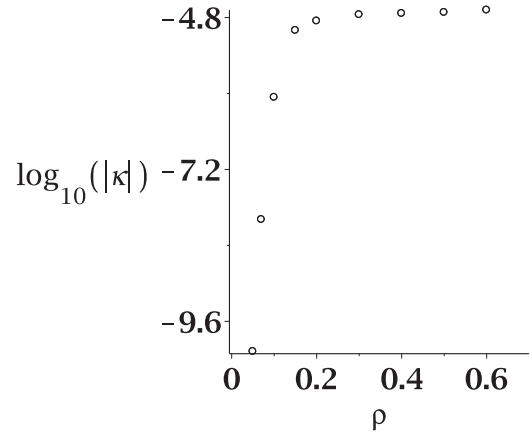


FIG. 9. Double slit: The behavior of the maximum value of the Sorkin parameter as a function of  $\rho_x$ . We used the set of parameters:  $\tau = 50$  ps,  $\sigma = 11.4 \mu\text{m}$ ,  $\Omega = \sigma \times 10^{E_{\mathcal{N}}}$ ,  $E_{\mathcal{N}} = 0.4$ ,  $\lambda = 702$  nm,  $d = 100 \mu\text{m}$ ,  $\beta = 5 \mu\text{m}$ .

We can see that the highest Sorkin parameter ( $\approx 10^{-4.8}$ ), is achieved for  $\rho_x(T) \geq 0.2$ .

Finally, one may construct other sets of nonclassical trajectories as shown in Fig. 10. Their contributions to the Sorkin parameter depends on the value of  $E_{\mathcal{N}}$  chosen. For a typical value of the ratio  $\Omega/\sigma \approx 100$  [51], yielding  $E_{\mathcal{N}} = 2$ , they are at least about eight orders of magnitude below the dominant contribution from the paths in Fig. 5. A reasonable rule of thumb is the more slits the photons go through, the lower their contribution.

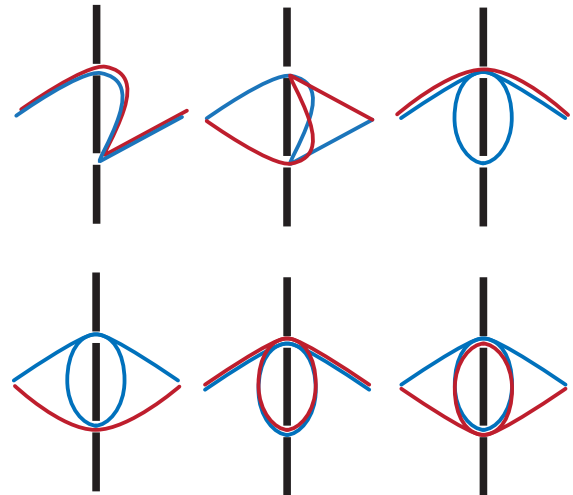


FIG. 10. Other types of nonclassical contributions to the wave function at the screen. Their contribution to the Sorkin parameter is at least around eight orders of magnitude lower than the one arising from paths in Fig. 5, for the same set of parameters used in Fig. 7 besides  $E_{\mathcal{N}} = 2$ . For this value of  $E_{\mathcal{N}}$ , the top left contribution is dominant and yields a Sorkin parameter of about  $10^{-15}$ . The top-right looped trajectory yields a Sorkin parameter of order  $10^{-16}$  for the same set of experimental values, placing looped trajectories in lower relevance as compared to kinked ones.

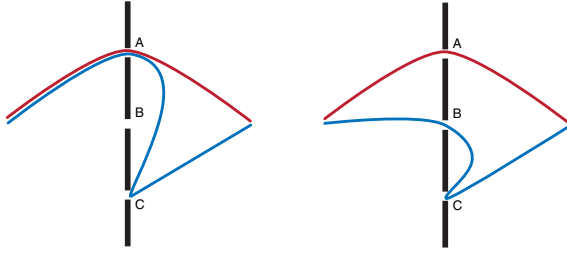


FIG. 11. Typical leading order contribution to nonclassical paths of biphotons.

**B. Sorkin parameter for the biphoton: Triple slit**

To evaluate the Sorkin parameter for light waves without any enhancement mechanism as in Ref. [15], triple-slit photon interference was described in Ref. [14,17,18].

The typical leading order contributions to nonclassical paths are depicted in Fig. 11. We adopt a set of parameters similar to those chosen in Ref. [14] as shown in Fig. 12. In addition, the value of  $\kappa$  is insensitive to whether coincidence measurements performed at the same point  $x_1 = x_2 = x$  or one detector is fixed at, say,  $x_2 = 0$ , and  $x_1 = x$  is an arbitrary point at the detection screen. In this optimized setup, the resulting Sorkin parameter is approximately  $10^{-5}$ . For  $E_{\mathcal{N}} = 2.0$ , the relevant nonclassical contributions come mainly from biphotons that pass through the same slit (paths like those on the left of Fig. 11). The Sorkin parameter is defined and evaluated in a similar fashion as for the double-slit case:

$$\kappa_{nc}(x_1, x_2) = \frac{I_{nc}(x_1, x_2) - I_c(x_1, x_2)}{I_{nc}(0, 0)}. \quad (42)$$

Figure 12 illustrates the profile of the Sorkin parameter for coincidence measurements for arbitrary  $x_1$  and  $x_2$ .

Curiously, and unlike the double-slit case shown in the previous section, the Sorkin parameter for coincidence measurements in a biphoton triple-slit setup is not as sensitive to the logarithmic negativity. There are no significant changes

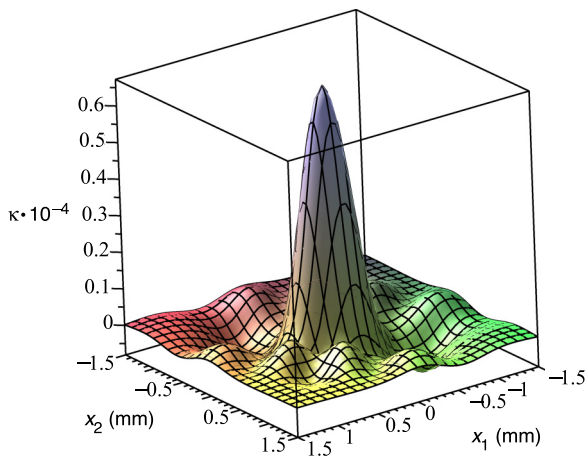


FIG. 12. Sorkin parameter for biphoton three-slit interference. We have adopted  $E_{\mathcal{N}} = 2.0$ ,  $T \approx 600$  ps for which  $\rho_x(600 \text{ ps}) = 0.026$ ,  $\sigma = 11.4 \mu\text{m}$ ,  $\lambda = 810 \text{ nm}$ ,  $\beta = 30 \mu\text{m}$ ,  $d = 100 \mu\text{m}$ ,  $\tau = T$ .

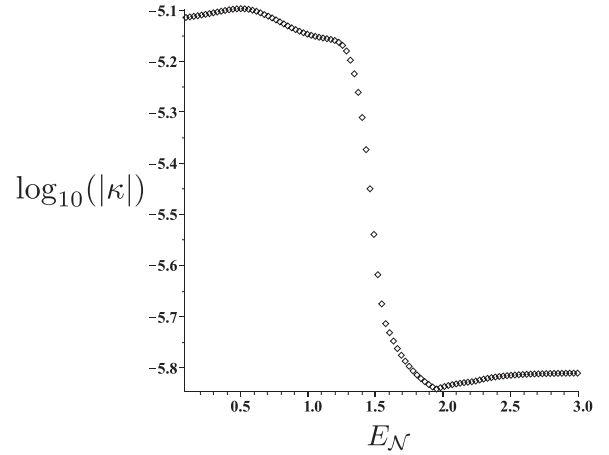


FIG. 13. Triple slit: Maximal Sorkin parameter for biphoton three-slit interference as a function of  $E_{\mathcal{N}}$ . We have adopted  $T \approx 60$  ps,  $\sigma = 11.4 \mu\text{m}$ ,  $\lambda = 810 \text{ nm}$ ,  $\beta = 10 \mu\text{m}$ ,  $d = 250 \mu\text{m}$ ,  $\tau = 270$  ps.

in the order of magnitude for the set of parameters we have chosen. However, for a different set of parameters as shown in Fig. 13, it displays a similar behavior as the double-slit for the maximum Sorkin parameter as a function of the negativity. The maximum value of  $\kappa$  is still around  $10^{-5}$  for  $E_{\mathcal{N}} = 0.5$ .

**C. Sorkin parameter for a massive particle**

*1. Triple-slit setup*

In this section, we will evaluate the Sorkin parameter for electron waves in a three-slit setup just as in Ref. [14] to assess the efficiency of our simplified model.

The effective propagator for a free particle of mass  $m$  reads [10]

$$G(x, t; x_0, t_0) = \sqrt{\frac{m}{2\pi i\hbar(t-t_0)}} \exp\left[\frac{-m(x-x_0)^2}{2i\hbar(t-t_0)}\right], \quad (43)$$

which was employed in Refs. [22,23,25] to study Gouy phases, matter wave interferometry, and exotic paths contributions to the Sorkin parameter.

Consider kinklike trajectories such as the one shown in Fig. 14 in which the slits are labeled A, B, and C.

A classical path amplitude contribution at the screen corresponding to, say, the particle going through the slit  $j$  reads

$$\psi_j(x) = \int_{x'',x'} G(x, T + \tau; x'', T) F_j(x'') G(x'', T; x', 0) \psi_0(x'), \quad (44)$$

where

$$\psi_0(x') = \frac{1}{\sqrt{\sigma_0\sqrt{\pi}}} \exp\left(-\frac{x'^2}{2\sigma_0^2}\right) \quad (45)$$

is the initial Gaussian wave packet, in which the standard deviation  $\sigma_0$  is related to the collimator size. The window functions  $F_j(x'')$  that modulate the slit apertures can be written as

$$F_{A,C}(x'') = e^{-\frac{(x'' \mp d)^2}{2\beta^2}} \quad \text{and} \quad F_B(x'') = e^{-\frac{x''^2}{2\beta^2}}. \quad (46)$$

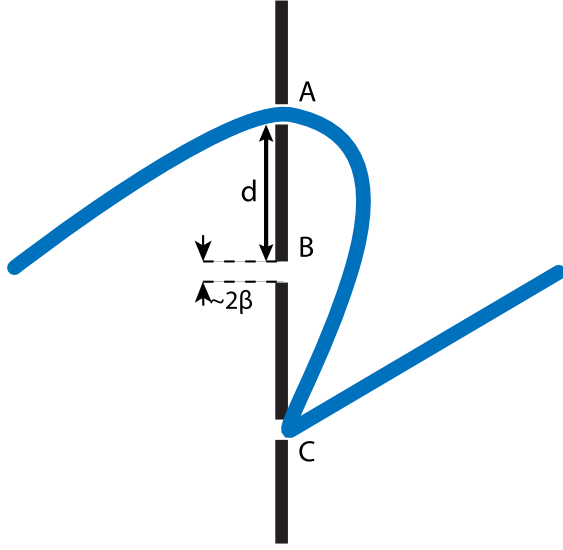


FIG. 14. An example of kink-type nonclassical trajectory in a three-slit Young experiment.

The nonclassical trajectory contributions are represented by  $\psi_{jl}$ , meaning the particle goes through slit  $j$ , then to slit  $l$ , then to the screen. They are evaluated as the following:

$$\begin{aligned} \psi_{jl}(x) = & \int_{x''', x'', x'} G(x, T + \delta + \tau; x''', T + \delta) \\ & \times F_l(x''') G(x'', T + \delta; x'', T) F_j(x'') \\ & \times G(x'', T; x', 0) \psi_0(x'), \end{aligned} \quad (47)$$

where the parameter  $\delta$  corresponds to the inter-slit transit time; for slits separated by  $d$  ( $2d$ ), it evaluates to  $\epsilon$  ( $2\epsilon$ ). The parameter  $\epsilon$  is evaluated using  $\epsilon = d/\Delta v_x$ , where  $\Delta v_x = \Delta p_x/m$ , in which  $\Delta p_x = \sqrt{\langle p_x^2 \rangle - \langle p_x \rangle^2}$  is the momentum variance orthogonal to the propagation direction.

We evaluate the Sorkin parameter following Ref. [17], as discussed in the Introduction. It reads

$$\kappa = \frac{\Delta I}{I_0}, \quad (48)$$

where, to first order in the path contributions,

$$\begin{aligned} \Delta I \approx 2\Re[\psi_A^*(\psi_{BC} + \psi_{CB}) + \psi_B^*(\psi_{AC} + \psi_{CA}) \\ + \psi_C^*(\psi_{AB} + \psi_{BA})], \end{aligned} \quad (49)$$

and  $I_0$  is the total intensity at the central peak. A plot of the Sorkin parameter for the parameters used for electron waves in Ref. [17] is found in Fig. 15. The order of magnitude obtained with our effective description agrees with the one obtained in Ref. [17], which validates our effective description.

## 2. Double-slit setup

It is instructive to rank the contributions to the Sorkin parameter in our framework for the interference one massive particle in a two-slit experiment arising from (a) nonclassical kink paths, (b) nonclassical looped path trajectories, and (c) relativistic corrections to the propagator. Because the contributions from nonclassical paths are very small, it is natural

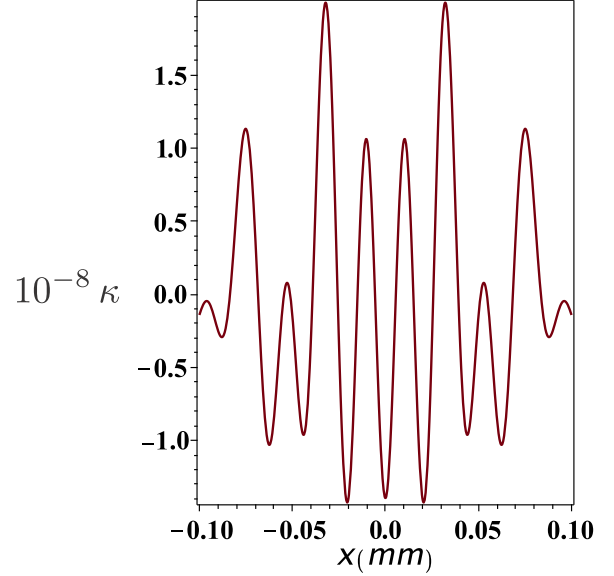


FIG. 15. The Sorkin parameter due to trajectories of type depicted in Fig. 14 in a three-slit setup. We have chosen to use an electron with de Broglie wavelength 50 pm,  $d = 272$  nm,  $\beta = 31$  nm, and  $\sigma_0 = 62$  nm. The source-to-slit distance is 24 cm, and the slits-to-screen one is 30.5 cm. The variable  $x$  is plotted in mm.

to ask how they compare to relativistic corrections, even for a small average velocities of particles (as compared to the speed of light) in the source beam.

Now let us proceed to rank the contributions of nonclassical paths (kinks or loops) for a double-slit setup as well as compare to relativistic corrections to the propagators. We shall use matter waves for neutrons and electrons.

Relativistic corrections can be implemented via a simple modification in the propagator as discussed in Ref. [59],

$$\begin{aligned} G_{\text{rel}}(x, t; x_0, t_0) = G(x, t; x_0, t_0) \left[ 1 - \frac{3(x - x_0)^2}{4c^2(t_E - t_{E_0})^2} \right. \\ \left. + \frac{m(x - x_0)^4}{8\hbar c^2(t_E - t_{E_0})^3} + O\left(\frac{1}{c^4}\right) \right], \end{aligned} \quad (50)$$

where  $G(x, t; x_0, t_0)$  is given by Eq. (43) and  $t_E$  stands for the Euclidian time, that is,  $t_E = it$ . Because the relativistic corrections are small, we will use them on the classical trajectories only. Hence, we have three distinct scenarios: (a) nonclassical kink-type trajectories, (b) nonclassical looped trajectories, and (c) relativistic corrections to the propagator.

The nonclassical kinklike trajectories are found in the same way as in Eq. (47). The loop contribution corresponding to a path such as in Fig. 1(b) is evaluated as

$$\begin{aligned} \psi_{\text{loop}-jk}(x) = & \int G(x, T + 2\epsilon + \tau; x''', T + 2\epsilon) F_j(x''') \\ & \times G(x''', T + 2\epsilon; x'', T + \epsilon) F_k(x'') \\ & \times G(x'', T + \epsilon; x', T) F_j(x') \\ & \times G(x'', T; x', 0) \psi_0(x'), \end{aligned} \quad (51)$$

which should be read as the particle goes first through slit  $j$ , then loops through slit  $k$ , and propagates from slit  $j$  to the

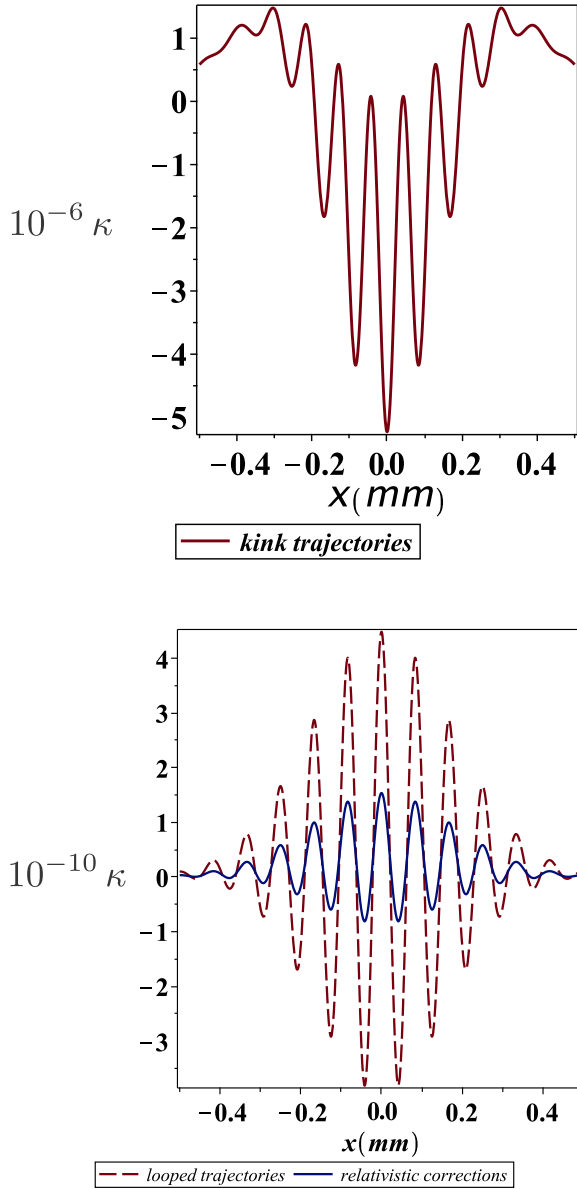


FIG. 16. The Sorkin parameter due to three different contributions for a neutron going through a double slit. The neutron has Broglie wavelength 2 nm, and the remaining parameters are  $d = 125 \mu\text{m}$ ,  $\beta = 7 \mu\text{m}$ ,  $\sigma_0 = 7 \mu\text{m}$ , and  $t = \tau = 26.4 \text{ ms}$ . For these parameters, the interslit transit time  $\epsilon$  is 18 ms. The variable  $x$  is plotted in mm. In this case, it is clear that the Sorkin parameter is generated mainly by kinklike trajectories, as the other contributions are about four orders of magnitude lower.

screen. The integrals are carried out over all primed coordinates  $\{x', x'', x''', x'''\}$ , and their analytical forms are shown in Appendix C. The relativistic corrections, on the other hand, are implemented by substituting the propagator in Eq. (44) by its corrected version in Eq. (50).

The Sorkin parameter is evaluated as shown in Eq. (30). Plots of the three scenarios are shown in Fig. 16, in which the parameters referring to a neutron were taken from Ref. [60]—the relativistic corrections were evaluated numerically. Clearly, the kink trajectories contribute more significantly, while the contributions from relativistic correc-

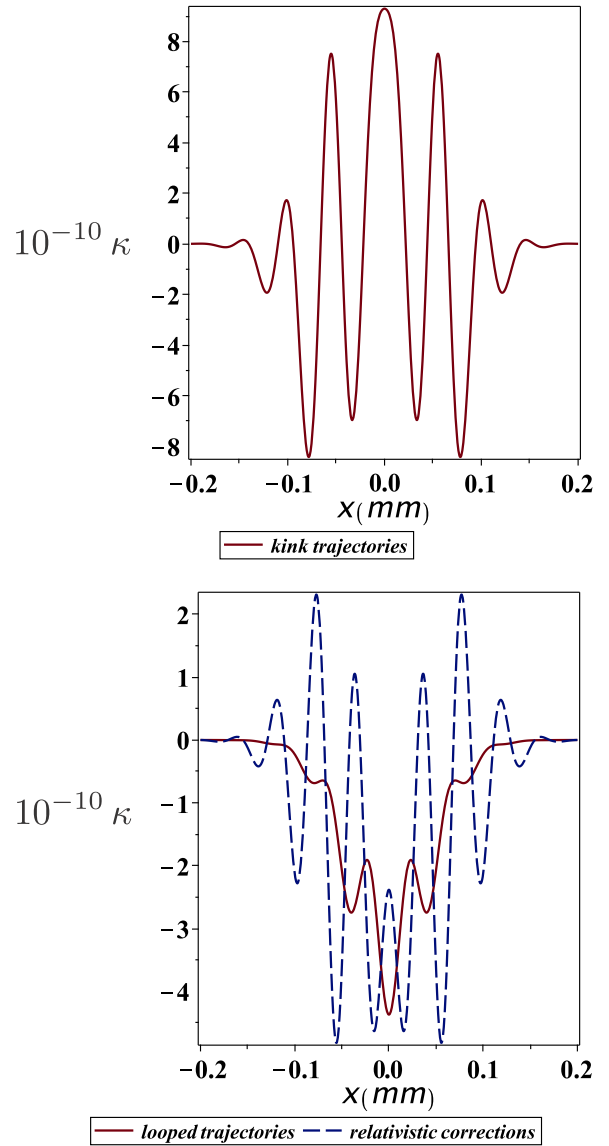


FIG. 17. The Sorkin parameter due to three different contributions for an electron going through a double slit. The electron has Broglie wavelength 50 pm, and the other relevant parameters are  $d = 272 \text{ nm}$ ,  $\beta = 62/2 \text{ nm}$ ,  $\sigma_0 = 62 \text{ nm}$ , and the source-slit (slit-screen) distance is 30.5 cm (24 cm). For these parameters, the interslit transit time  $\epsilon$  is 0.1 ns. The variable  $x$  is plotted in mm.

tions and looped trajectories are of comparable magnitude. In Fig. 17, similar computations were carried out for an electron, in which one can see this hierarchy is such that the kink contributions are still the largest by about one order of magnitude in comparison with looped path contributions, which compete with the relativistic corrections.

### V. CONCLUSIONS AND FINAL REMARKS

The study of nonclassical or exotic paths contributions to interferometry of light and matter waves evolved along endeavors to measure deviations from Born’s rule and the superposition principle in interference experiments. While in theory the answer is very simple, as encoded in the Feynman

path integral formalism, the boundary conditions involved in the computation of multislit diffractions with exotic paths are overwhelmingly difficult and require sophisticated computational resources. Moreover, for light waves, the absence of a time-dependent formalism to calculate single-particle diffraction and issues with photon localization begs for an effective description of the problem. For example, under the scalar wave approximation, the propagation of light is described by the Helmholtz equation subjected to adequate boundary conditions. Thus, an effective propagator that satisfies the Fresnel-Huygens principle can be used to compute nonclassical trajectories using numerical integration and resource intensive FDTD simulations. Orders of magnitude predicted by theoretical predictions are valuable guides for experimentalists and are worth exploring. Using an effective double Gaussian approximation for describing type-I SPDC biphotons and the Fresnel approximation to build an effective propagator, we have computed the leading order contributions for biphoton interference in double- and triple-slit setups. We have obtained that the Sorkin parameter  $\kappa$  can be of order  $10^{-5}$ , which is one order of magnitude larger than typical photon experiments to determine  $\kappa$ . We have found that the spatial correlations encoded in the double Gaussian parameters may play a significant role in the double-slit setup. Moreover, we have explicitly demonstrated that our simple mathematical model, which can be evaluated using MAPLE, reproduces the order of magnitude of the Sorkin parameter for matter waves, such as the electron, for the same set of parameters used in other simulations. Finally, we have addressed the question about the hierarchy of contributing nonclassical paths to the Sorkin parameter. We found that kink-shaped paths are of course the leading contributions and that looped paths can contribute with the same order of magnitude as relativistic corrections to the propagator.

#### ACKNOWLEDGMENTS

F.C.V.B. and C.H.S.V. thank Coordenação de Aperfeiçoamento de Pessoal de Nível Superior (CAPES). I.G.P. thanks Conselho Nacional de Desenvolvimento Científico e Tecnológico (CNPq), Grant No. 307942/2019-8. J.B.A. thanks CNPq for Grant No. 150190/2019-0, and M.S. thanks CNPq for Grant No. 303482/2017-6.

#### APPENDIX A: BIPHOTON CLASSICAL WAVE-FUNCTION CONSTANTS

The general form of a classical trajectory wave function at the screen (see Sec. III) is

$$\psi_i = A \exp [C_i(r, q) + i\alpha_i(r, q)], \quad (\text{A1})$$

with

$$\begin{aligned} C &\equiv c_1 r^2 + c_2 q^2 + c_3 r + c_4 q + c_5, \\ \alpha &\equiv a_1 r^2 + a_2 q^2 + a_3 r + a_4 q + a_5. \end{aligned} \quad (\text{A2})$$

Please note we have intentionally dropped the index  $i$ , the reason for it will be clear below. The coefficients are given by

$$c_1 = -\left(\frac{4\pi^2}{\lambda^2 c^2 \tau^2}\right) \text{Re} \left[ \frac{1}{\omega} \right], \quad (\text{A3})$$

$$c_2 = -\left(\frac{4\pi^2}{\lambda^2 c^2 \tau^2}\right) \text{Re} \left[ \frac{1}{\Sigma} \right], \quad (\text{A4})$$

$$c_3 = -\frac{\pi}{\lambda c \tau} \left(\frac{d_1 + d_2}{\beta^2}\right) \text{Im} \left[ \frac{1}{\omega} \right], \quad (\text{A5})$$

$$c_4 = \frac{\pi}{\lambda c \tau} \left(\frac{d_1 - d_2}{\beta^2}\right) \text{Im} \left[ \frac{1}{\Sigma} \right], \quad (\text{A6})$$

$$c_5 = -\frac{(d_1^2 + d_2^2)}{8\beta^2} - \frac{(d_1 + d_2)^2}{4\beta^4} \text{Re} \left[ \frac{1}{4\omega} \right] \quad (\text{A7})$$

$$+ \frac{(-d_1 + d_2)^2}{\beta^4} \text{Re} \left[ \frac{1}{4\Sigma} \right], \quad (\text{A8})$$

$$a_1 = \frac{2\pi}{\lambda c \tau} + \left(\frac{4\pi^2}{\lambda^2 c^2 \tau^2}\right) \text{Im} \left[ \frac{1}{\omega} \right], \quad (\text{A9})$$

$$a_2 = \frac{2\pi}{\lambda c \tau} + \left(\frac{4\pi^2}{\lambda^2 c^2 \tau^2}\right) \text{Im} \left[ \frac{1}{\Sigma} \right], \quad (\text{A10})$$

$$a_3 = -\frac{\pi}{\lambda c \tau} \frac{(d_1 + d_2)}{\beta^2} \text{Re} \left[ \frac{1}{\omega} \right], \quad (\text{A11})$$

$$a_4 = \frac{\pi}{\lambda c \tau} \frac{(d_1 - d_2)}{\beta^2} \text{Re} \left[ \frac{1}{\Sigma} \right], \quad (\text{A12})$$

and  $a_5$  is given by

$$a_5 = \theta + \zeta, \quad (\text{A13})$$

where

$$\theta = -\frac{(d_1 + d_2)^2}{4\beta^4} \text{Im} \left[ \frac{1}{4\omega} \right] + \frac{(-d_1 + d_2)^2}{\beta^4} \text{Im} \left[ \frac{1}{4\Sigma} \right], \quad (\text{A14})$$

$$\zeta = \frac{1}{2} \arctan \left( \frac{\text{Im}[\omega\Sigma]}{\text{Re}[\omega\Sigma]} \right), \quad (\text{A15})$$

in which

$$\omega = \frac{1}{\beta^2} + \frac{2\pi}{I\lambda c \tau} + \frac{1}{\Omega^2 + I\frac{\lambda c \tau}{2\pi\Omega}}, \quad (\text{A16})$$

$$\Sigma = \frac{1}{\beta^2} + \frac{2\pi}{I\lambda c \tau} + \frac{1}{\sigma^2 + I\frac{\lambda c \tau}{2\pi\sigma}}. \quad (\text{A17})$$

TABLE I. Choices of  $d_{1,2}$  corresponding to the biphoton's four classical trajectories.

$i$	$d_1$	$d_2$
$uu$	$-d$	$-d$
$dd$	$d$	$d$
$ud$	$-d$	$d$
$du$	$d$	$-d$

The amplitude, which is the same for all classical trajectories, is given by

$$A = \left( \frac{\pi}{\lambda c \tau} \right) \frac{1}{\sqrt{\pi |\omega| |\Sigma| |\sigma + i\alpha/\sigma| |\Omega + i\alpha/\Omega|}}, \quad (\text{A18})$$

where  $\alpha = \lambda c t / 2\pi$ .

Now that the coefficients were stated, the index  $i$  in Eq. (A1) will tell us which values of  $d_{1,2}$  one should take in Eqs. (A5)–(A7) and (A11)–(A14). As  $i = \{uu, dd, ud, du\}$ , Table I displays the choices of  $d_{1,2}$  corresponding to each of the four classical contributions.

In our numerical evaluations for the plots, since we are interested in the interference pattern, we have disregarded the factor  $\sqrt{\frac{\hbar}{2\pi i \hbar(t-i)}}$  in the propagator of Eq. (16).

## APPENDIX B: BIPHOTON NONCLASSICAL WAVE-FUNCTION CONSTANTS

The general form of the nonclassical trajectory wave function at the screen (see Sec. IV A.) is given by

$$\psi_{\text{nc}(a_i, b_i)}(x_1, x_2) = A_{\text{nc}(a_i, b_i)} \exp[C_{\text{nc}(a_i, b_i)}(x_1, x_2) + i \alpha_{\text{nc}(a_i)}(x_1, x_2)], \quad (\text{B1})$$

where the coefficients  $C_{\text{nc}(a_i, b_i)}(x_1, x_2)$  and  $\alpha_{\text{nc}(a_i, b_i)}(x_1, x_2)$ , omitting the  $i$  index, have the general form

$$C_{\text{nc}(a, b)} \equiv \bar{c}_1 x_1^2 + \bar{c}_2 x_2^2 + \bar{c}_3 x_1 x_2 + \bar{c}_4 x_1 + \bar{c}_5 x_2 + \bar{c}_6, \quad \alpha_{\text{nc}(a, b)} \equiv \bar{a}_1 x_1^2 + \bar{a}_2 x_2^2 + \bar{a}_3 x_1 x_2 + \bar{a}_4 x_1 + \bar{a}_5 x_2 + \bar{a}_6. \quad (\text{B2})$$

The coefficients are given by

$$\bar{c}_1 = -\left( \frac{\pi^2}{\lambda^2 c^2 \tau^2} \right) \text{Re} \left[ \frac{1}{\chi_1} \right], \quad (\text{B3})$$

$$\bar{c}_2 = -\left( \frac{\pi}{\lambda c \tau} \right)^2 \text{Re} \left[ \frac{1}{\chi_2} \right] + \left( \frac{\pi^2 \Theta}{2\lambda^2 c^2 \tau \epsilon} \right)^2 \text{Re} \left[ \frac{1}{\chi_1 \chi_2^2 \chi_3^2} \right], \quad (\text{B4})$$

$$\bar{c}_3 = -\frac{\pi^3}{\lambda^3 c^3 \tau^2 \epsilon} \text{Im} \left[ \frac{1}{\chi_1 \chi_2 \chi_3} \right], \quad (\text{B5})$$

$$\bar{c}_4 = \frac{\pi^2 d_3}{2\lambda c \tau \beta^2} \text{Im} \left[ \frac{1}{\chi_1} \right] - \frac{\pi^2 \Theta}{4\lambda^2 c^2 \tau \beta^2} \left( \frac{d_1}{\tau} + \frac{d_2}{\epsilon} \right) \text{Re} \left[ \frac{1}{\chi_1 \chi_2 \chi_3} \right] + \frac{\pi^2 \Theta^2 d_1}{8\lambda^2 c^2 \tau^2 \beta^2} \text{Re} \left[ \frac{1}{\chi_1 \chi_2 \chi_3^2} \right], \quad (\text{B6})$$

$$\bar{c}_5 = \frac{\pi d_2}{2\lambda c \tau \beta^2} \text{Im} \left[ \frac{1}{\chi_2} \right] - \frac{\pi^3 \Theta^2}{8\lambda^3 c^3 \tau \epsilon \beta^2} \left( \frac{d_1}{\tau} + \frac{d_2}{\epsilon} \right) \text{Im} \left[ \frac{1}{\chi_1 \chi_2^2 \chi_3^2} \right] + \frac{\pi^3 \Theta^3 d_1}{16\lambda^3 c^3 \tau \epsilon^2 \beta^2} \text{Im} \left[ \frac{1}{\chi_1 \chi_2^2 \chi_3^3} \right] - \frac{\pi^2 d_3}{4\lambda^2 c^2 \tau \epsilon \beta^2} \text{Re} \left[ \frac{1}{\chi_1 \chi_2 \chi_3} \right], \quad (\text{B7})$$

$$\begin{aligned} \bar{c}_6 = & \frac{1}{8\beta^2} (d_1^2 + d_2^2 + d_3^2) + \frac{1}{16\beta^4} \text{Re} \left[ \frac{d_1^2}{\chi_3} + \frac{d_2^2}{\chi_2} + \frac{d_3^2}{\chi_1} \right] + \frac{\pi \Theta d_3}{16\lambda c \beta^4} \left( \frac{d_1}{\tau} + \frac{d_2}{\epsilon} \right) \text{Im} \left[ \frac{1}{\chi_1 \chi_2 \chi_3} \right] \\ & + \frac{\pi^2 \Theta^3 d_1}{64\lambda^2 c^2 \epsilon \beta^4} \left( \frac{d_1}{\tau} + \frac{d_2}{\epsilon} \right) \text{Re} \left[ \frac{1}{\chi_1 \chi_2^2 \chi_3^3} \right] - \frac{\pi^2 \Theta^2}{64\lambda^2 c^2 \beta^4} \left( \frac{d_1}{\tau} + \frac{d_2}{\epsilon} \right)^2 \text{Re} \left[ \frac{1}{\chi_1 \chi_2^2 \chi_3^2} \right] - \frac{\pi d_1 d_3 \Theta^2}{32\lambda c \epsilon \beta^4} \text{Im} \left[ \frac{1}{\chi_1 \chi_2 \chi_3^2} \right] \\ & - \frac{\pi^2 d_1^2 \Theta^4}{4 \cdot 64\lambda^2 c^2 \epsilon^2 \beta^4} \text{Re} \left[ \frac{1}{\chi_1 \chi_2^2 \chi_3^4} \right], \end{aligned} \quad (\text{B8})$$

$$\bar{a}_1 = \frac{\pi}{\lambda c \tau} + \left( \frac{\pi^2}{\lambda^2 c^2 \tau^2} \right) \text{Im} \left[ \frac{1}{\chi_1} \right], \quad (\text{B9})$$

$$\bar{a}_2 = \frac{\pi}{\lambda c \tau} + \left( \frac{\pi^2}{\lambda^2 c^2 \tau^2} \right) \text{Im} \left[ \frac{1}{\chi_2} \right] - \left( \frac{\pi^2 \Theta}{2\lambda^2 c^2 \tau \epsilon} \right)^2 \text{Im} \left[ \frac{1}{\chi_1 \chi_2^2 \chi_3^2} \right], \quad (\text{B10})$$

$$\bar{a}_3 = -\frac{\pi^3}{\lambda^3 c^3 \tau^2 \epsilon} \text{Re} \left[ \frac{1}{\chi_1 \chi_2 \chi_3} \right], \quad (\text{B11})$$

$$\bar{a}_4 = \frac{\pi^2 d_3}{2\lambda c \tau \beta^2} \text{Re} \left[ \frac{1}{\chi_1} \right] - \frac{\pi^2 \Theta}{4\lambda^2 c^2 \tau \beta^2} \left( \frac{d_1}{\tau} + \frac{d_2}{\epsilon} \right) \text{Im} \left[ \frac{1}{\chi_1 \chi_2 \chi_3} \right] - \frac{\pi^2 \Theta^2 d_1}{8\lambda^2 c^2 \tau^2 \beta^2} \text{Im} \left[ \frac{1}{\chi_1 \chi_2 \chi_3^2} \right], \quad (\text{B12})$$

$$\bar{a}_5 = \frac{\pi d_2}{2\lambda c \tau \beta^2} \text{Re} \left[ \frac{1}{\chi_2} \right] + \frac{\pi^3 \Theta^2}{8\lambda^3 c^3 \tau \epsilon \beta^2} \left( \frac{d_1}{\tau} + \frac{d_2}{\epsilon} \right) \text{Re} \left[ \frac{1}{\chi_1 \chi_2^2 \chi_3^2} \right] + \frac{\pi^3 \Theta^3 d_1}{16\lambda^3 c^3 \tau \epsilon^2 \beta^2} \text{Re} \left[ \frac{1}{\chi_1 \chi_2^2 \chi_3^3} \right] + \frac{\pi^2 d_3}{4\lambda^2 c^2 \tau \epsilon \beta^2} \text{Im} \left[ \frac{1}{\chi_1 \chi_2 \chi_3} \right], \quad (\text{B13})$$

and  $\bar{a}_6 = \bar{\theta} + \bar{\zeta}$

$$\bar{\theta} = -\frac{1}{16\beta^4} \text{Im} \left[ \frac{d_1^2}{\chi_3} + \frac{d_2^2}{\chi_2} + \frac{d_3^2}{\chi_1} \right] + \frac{\pi \Theta d_3}{16\lambda c \beta^4} \left( \frac{d_1}{\tau} + \frac{d_2}{\epsilon} \right) \text{Re} \left[ \frac{1}{\chi_1 \chi_2 \chi_3} \right] - \frac{\pi^2 \Theta^3 d_1}{64\lambda^2 c^2 \epsilon \beta^4} \left( \frac{d_1}{\tau} + \frac{d_2}{\epsilon} \right) \text{Im} \left[ \frac{1}{\chi_1 \chi_2^2 \chi_3^3} \right] \\ + \frac{\pi^2 \Theta^2}{64\lambda^2 c^2 \beta^4} \left( \frac{d_1}{\tau} + \frac{d_2}{\epsilon} \right)^2 \text{Im} \left[ \frac{1}{\chi_1 \chi_2^2 \chi_3^2} \right] - \frac{\pi d_1 d_3 \Theta^2}{32\lambda c \epsilon \beta^4} \text{Re} \left[ \frac{1}{\chi_1 \chi_2 \chi_3^2} \right] + \frac{\pi^2 d_1^2 \Theta^4}{4 \cdot 64\lambda^2 c^2 \epsilon^2 \beta^4} \text{Im} \left[ \frac{1}{\chi_1 \chi_2^2 \chi_3^4} \right], \quad (\text{B14})$$

$$\bar{\zeta} = -\frac{1}{2} \arctan \left( \frac{\text{Re}[\chi_1 \chi_2 \chi_3]}{\text{Im}[\chi_1 \chi_2 \chi_3]} \right), \quad (\text{B15})$$

where

$$\chi_1 = \frac{1}{2\beta^2} + \frac{\pi}{I\lambda c \epsilon} + \frac{\pi}{I\lambda c \tau} + \frac{\pi}{\lambda^2 c^2 \epsilon^2 \chi_3} + \frac{\pi^2 \Theta^2}{4\lambda^2 c^2 \epsilon^2 \chi_2 \chi_3^2}, \quad (\text{B16})$$

$$\chi_2 = \frac{1}{2\beta^2} + \frac{\pi}{I\lambda c \tau} + \frac{1}{\Omega^2 + I\frac{\lambda c t}{2\pi}} + \frac{1}{\sigma^2 + I\frac{\lambda c t}{2\pi}} - \frac{\Theta^2}{4\chi_3}, \quad (\text{B17})$$

$$\chi_3 = \frac{1}{2\beta^2} + \frac{\pi}{I\lambda c \epsilon} + \frac{1}{\Omega^2 + I\frac{\lambda c t}{2\pi}} + \frac{1}{\sigma^2 + I\frac{\lambda c t}{2\pi}}, \quad (\text{B18})$$

where  $\Theta = \left( \frac{1}{\Omega^2 + iI\frac{\lambda c t}{2\pi}} - \frac{1}{\sigma^2 + I\frac{\lambda c t}{2\pi}} \right)$ .

The amplitude is given by

$$A_{\text{nc}(a,b)} = \frac{1}{\sqrt{\pi} |\omega| |\Sigma| |\sigma + i\alpha/\sigma| |\Omega + i\alpha/\Omega|} \frac{\pi^{3/2}}{\lambda c \sqrt{\epsilon \tau} |\chi_1 \chi_2 \chi_3|}, \quad (\text{B19})$$

where  $\alpha = \lambda c t / 2\pi$ .

Now that the coefficients were stated, Table II will tell us which values of  $d_{1,2,3}$  one should take in Eqs. (B6)–(B8) and (B12)–(B14).

It is clear that  $\psi_{\text{nc}(a_2)}$  and  $\psi_{\text{nc}(a_4)}$  ( $\psi_{\text{nc}(b_2)}$  and  $\psi_{\text{nc}(b_4)}$ ), are symmetric under particle exchange to  $\psi_{\text{nc}(a_1)}$  and  $\psi_{\text{nc}(a_3)}$  ( $\psi_{\text{nc}(b_1)}$  and  $\psi_{\text{nc}(b_3)}$ ), respectively, as shown in Figs. 5 and 6. This means that to obtain  $\psi_{\text{nc}(a_2)}$  and  $\psi_{\text{nc}(a_4)}$  ( $\psi_{\text{nc}(b_2)}$  and  $\psi_{\text{nc}(b_4)}$ ), we just have to interchange  $x_1$  and  $x_2$  in  $\psi_{\text{nc}(a_1)}$  and  $\psi_{\text{nc}(a_3)}$  ( $\psi_{\text{nc}(b_1)}$  and  $\psi_{\text{nc}(b_3)}$ ), respectively.

### APPENDIX C: WAVE-FUNCTION CONSTANTS FOR A MASSIVE PARTICLE DIFFRACTING THROUGH A DOUBLE SLIT

#### 1. Classical path wave-function constants

Considering a double slit, which has its slits labeled A and B, one can obtain the wave function related to the classical propagation solving Eq. (44), with the slit function given by  $F_{A,B} = e^{-\frac{(\chi' \mp d/2)^2}{2\beta^2}}$ . The wave function that describes the particle leaving the source, going through the upper slit (slit A) and

reaching the screen can be written as

$$\psi_A(x) = \frac{1}{\sqrt{\beta} \sqrt{\pi}} \exp \left[ -\frac{(x - D_A/2)^2}{2B_A^2} \right] \\ \times \exp \left( \frac{imx^2}{2\hbar R_A} - i\Delta_A x + i\theta_A + i\mu_A \right), \quad (\text{C1})$$

where

$$B_A^2(t, \tau) = \frac{\left( \frac{1}{\beta^2} + \frac{1}{b^2} \right)^2 + \frac{m^2}{\hbar^2} \left( \frac{1}{\tau} + \frac{1}{r} \right)^2}{\left( \frac{m}{\hbar \tau} \right)^2 \left( \frac{1}{\beta^2} + \frac{1}{b^2} \right)}, \quad (\text{C2})$$

$$R_A(t, \tau) = \tau \frac{\left( \frac{1}{\beta^2} + \frac{1}{b^2} \right)^2 + \frac{m^2}{\hbar^2} \left( \frac{1}{\tau} + \frac{1}{r} \right)^2}{\left( \frac{1}{\beta^2} + \frac{1}{b^2} \right) + \left( \frac{t}{\sigma_0 b^2} \right) \left( \frac{1}{\tau} + \frac{1}{r} \right)}, \quad (\text{C3})$$

$$D_A(t, \tau) = \frac{\left( 1 + \frac{t}{r} \right)}{\left( 1 + \frac{\beta^2}{b^2} \right)} d, \quad (\text{C4})$$

$$\Delta_A(t, \tau) = \frac{\tau \sigma_0^2 d}{2\tau_0 \beta^2 B_A^2}, \quad (\text{C5})$$

$$\theta_A(t, \tau) = \frac{m d^2 \left( \frac{1}{\tau} + \frac{1}{r} \right)}{8\hbar \beta^4 \left[ \left( \frac{1}{\beta^2} + \frac{1}{b^2} \right)^2 + \frac{m^2}{\hbar^2} \left( \frac{1}{\tau} + \frac{1}{r} \right)^2 \right]}, \quad (\text{C6})$$

$$\mu_A(t, \tau) = -\frac{1}{2} \arctan \left[ \frac{t + \tau \left( 1 + \frac{\sigma_0^2}{\beta^2} \right)}{\tau_0 \left( 1 - \frac{t\tau \sigma_0^2}{\tau_0^2 \beta^2} \right)} \right], \quad (\text{C7})$$

$$b^2(t) = \sigma_0^2 \left[ 1 + \left( \frac{t}{\tau_0} \right)^2 \right], \quad (\text{C8})$$

and

$$r(t) = t \left[ 1 + \left( \frac{\tau_0}{t} \right)^2 \right]. \quad (\text{C9})$$

Here, the parameter  $B_A^2(t, \tau)$  is the beam width for the propagation through one slit,  $R_A(t, \tau)$  is the radius of curvature of the wavefronts for the propagation through one slit,  $b(t)$  is the beam width for the free propagation, and  $r(t)$  is the radius of curvature of the wavefronts for the free propagation.

TABLE II. Choices of  $d_{1,2,3}$  corresponding to the biphoton's exotic trajectories.

$\psi_{\text{nc}}$	$d_1$	$d_2$	$d_3$
$\psi_{\text{nc}(a_1)}$	$-d$	$-d$	$d$
$\psi_{\text{nc}(a_3)}$	$d$	$d$	$-d$
$\psi_{\text{nc}(b_1)}$	$-d$	$d$	$d$
$\psi_{\text{nc}(b_3)}$	$d$	$-d$	$-d$

$D_A(t, \tau)$  is the separation between the wave packets produced in the double slit.  $\Delta_A(t, \tau)x$  is a phase which varies linearly with the transverse coordinate.  $\theta_A(t, \tau)$  and  $\mu_A(t, \tau)$  are the time-dependent phases and they are relevant only if the slits have different widths.  $\mu_A(t, \tau)$  is the Gouy phase for the propagation through one slit.  $\tau_0 = \frac{m\sigma_0^2}{\hbar}$  is the characteristic time for the aging of the initial state. The wave function for the propagation going through slit B can be obtained replacing  $d$  with  $-d$  in Eqs. (C4)–(C6).

**2. Kink path wave-function constants**

The wave function for a massive particle performing a kink ( $k$ ) trajectory through a double slit can be computed by solving the Eq. (47), with the slit function given by  $F_{A,B} = e^{-\frac{(x' \mp d/2)^2}{2\beta^2}}$ . Considering the propagation that goes from slit A (upper slit) to the slit B (lower slit), the corresponding wave function can be written as

$$\psi_{AB} = A_k \exp [C_k(x) + i\alpha_k(x)], \tag{C10}$$

where

$$C_k \equiv c'_1 x^2 + c'_2 x + c'_3, \tag{C11}$$

$$\alpha_k \equiv a'_1 x^2 + a'_2 x + a'_3, \tag{C12}$$

$$c'_1 = -\frac{m^2}{4\hbar^2 \tau^2} \operatorname{Re} \left[ \frac{1}{\Gamma_3} \right], \tag{C13}$$

$$c'_2 = \frac{md}{4\hbar \tau \beta^2} \operatorname{Im} \left[ \frac{1}{\Gamma_3} \right] - \frac{m^2 d}{8\hbar^2 \tau \epsilon \beta^2} \operatorname{Re} \left[ \frac{1}{\Gamma_2 \Gamma_3} \right], \tag{C14}$$

$$c'_3 = -\frac{d^2}{4\beta^2} + \frac{d^2}{16\beta^4} \operatorname{Re} \left[ \frac{1}{\Gamma_2} \right] + \frac{d^2}{16\beta^4} \operatorname{Re} \left[ \frac{1}{\Gamma_3} \right] + \frac{d^2}{16\hbar \epsilon \beta^4} \operatorname{Im} \left[ \frac{1}{\Gamma_2 \Gamma_3} \right] - \frac{d^2}{64\hbar^2 \epsilon^2 \beta^4} \operatorname{Im} \left[ \frac{1}{\Gamma_2^2 \Gamma_3} \right],$$

$$a'_1 = \frac{m}{2\hbar \tau} + \frac{m^2}{4\hbar^2 \tau^2} \operatorname{Im} \left[ \frac{1}{\Gamma_3} \right], \tag{C15}$$

$$a'_2 = \frac{md}{4\hbar \tau \beta^2} \operatorname{Re} \left[ \frac{1}{\Gamma_3} \right] + \frac{m^2 d}{8\hbar^2 \tau \beta^2} \operatorname{Im} \left[ \frac{1}{\Gamma_2 \Gamma_3} \right], \tag{C16}$$

and  $a'_3 = \theta' + \mu$ , where

$$\theta' = -\frac{d^2}{16\beta^4} \operatorname{Im} \left[ \frac{1}{\Gamma_2} \right] - \frac{d^2}{16\beta^4} \operatorname{Im} \left[ \frac{1}{\Gamma_3} \right] + \frac{md^2}{16\hbar \epsilon \beta^4} \operatorname{Re} \left[ \frac{1}{\Gamma_2 \Gamma_3} \right] + \frac{m^2 d^2}{64\hbar^2 \epsilon^2 \beta^4} \operatorname{Im} \left[ \frac{1}{\Gamma_2^2 \Gamma_3} \right], \tag{C17}$$

$$\mu' = -\frac{1}{2} \arctan \left( \frac{\operatorname{Im}[\Gamma_1 \Gamma_2 \Gamma_3]}{\operatorname{Re}[\Gamma_1 \Gamma_2 \Gamma_3]} \right), \tag{C18}$$

in which

$$\Gamma_1 = \frac{1}{2\sigma_0^2} + \frac{Im}{2\hbar t}, \tag{C19}$$

$$\Gamma_2 = \frac{1}{2\beta^2} + \frac{Im}{2\hbar t} + \frac{Im}{2\hbar \epsilon} + \frac{m^2}{4\hbar^2 t^2 \Gamma_1}, \tag{C20}$$

$$\Gamma_3 = \frac{1}{2\beta^2} + \frac{Im}{2\hbar \epsilon} + \frac{Im}{2\hbar \tau} + \frac{m^2}{4\hbar^2 \epsilon^2 \Gamma_2}. \tag{C21}$$

The amplitude is given by

$$A_k = \frac{1}{\sqrt{\sigma_0 \sqrt{\pi}}} \left( \frac{m}{2\hbar} \right)^{3/2} \frac{1}{\sqrt{t \epsilon \tau |\Gamma_1 \Gamma_2 \Gamma_3|}}. \tag{C22}$$

The wave function  $\psi_{BA}$  for the propagation going through slit B, then to slit A, can be obtained replacing  $d$  with  $-d$  in Eqs. (C13) and (C16).

**3. Loop path wave-function constants**

After some manipulation, Eq. (51) gives the wave function that describes a loop propagation ( $l$ ) through a double slit, with the slit function given by  $F_{A,B} = e^{-\frac{(x' \mp d/2)^2}{2\beta^2}}$ . The state for a massive particle propagating first through slit A (upper slit), then loops through slit B (lower), and propagates from slit A to the screen is given by

$$\psi_{\text{loop-}AB} = A_l \exp [C_l(x) + i\alpha_l(x)], \tag{C23}$$

with

$$C_l \equiv c''_1 x^2 + c''_2 x + c''_3, \quad \alpha_l \equiv a''_1 x^2 + a''_2 x + a''_3, \tag{C24}$$

where

$$c''_1 = -\frac{m^2}{4\hbar^2 \tau^2} \operatorname{Re} \left[ \frac{1}{\gamma_3} \right], \tag{C25}$$

$$c''_2 = -\frac{md}{4\beta^2 \hbar \tau} \operatorname{Im} \left[ \frac{1}{\gamma_3} \right] + \frac{m^2 d}{16\beta^2 \hbar^2 \tau \epsilon} \operatorname{Re} \left[ \frac{1}{\gamma_2 \gamma_3} \right] + \frac{m^3 d}{64\beta^2 \hbar^3 \tau \epsilon^2} \operatorname{Im} \left[ \frac{1}{\gamma_1 \gamma_2 \gamma_3} \right], \tag{C26}$$

$$c''_3 = -\frac{3d^2}{8\beta^2} + \frac{d^2}{16\beta^4} \operatorname{Re} \left[ \frac{1}{\gamma_1} \right] + \frac{d^2}{16\beta^4} \operatorname{Re} \left[ \frac{1}{\gamma_2} \right] + \frac{d^2}{16\beta^4} \operatorname{Re} \left[ \frac{1}{\gamma_3} \right] - \frac{m^2 d^2}{4^4 \beta^4 \hbar^2 \epsilon^2} \operatorname{Re} \left[ \frac{1}{\gamma_1 \gamma_2} \right] + \frac{m^4 d^2}{4^6 \beta^4 \hbar^4 \epsilon^2} \operatorname{Re} \left[ \frac{1}{\gamma_1^2 \gamma_2^2 \gamma_3} \right] - \frac{m^2 d^2}{2^7 \beta^4 \hbar^2 \epsilon^2} \operatorname{Re} \left[ \frac{1}{\gamma_1 \gamma_2 \gamma_3} \right] - \frac{md^2}{32\beta^4 \hbar \epsilon} \operatorname{Re} \left[ \frac{1}{\gamma_1 \gamma_2} + \frac{1}{\gamma_2 \gamma_3} \right] - \frac{m^2 d^2}{4^4 \beta^4 \hbar^2 \epsilon^2} \operatorname{Re} \left[ \frac{1}{\gamma_2^2 \gamma_3} \right] - \frac{m^3 d^2}{2^9 \beta^4 \hbar^3 \epsilon^3} \operatorname{Im} \left[ \frac{1}{\gamma_1 \gamma_2^2 \gamma_3} \right], \tag{C27}$$



$$a_1'' = \frac{m}{2\hbar\tau} + \frac{m^2}{4\hbar\tau^2} \text{Im} \left[ \frac{1}{\gamma_3} \right], \quad (\text{C28})$$

$$a_2'' = -\frac{md}{4\beta^2\hbar\tau} \text{Re} \left[ \frac{1}{\gamma_3} \right] + \frac{m^2d}{16\beta^2\hbar\tau\epsilon} \text{Im} \left[ \frac{1}{\gamma_2\gamma_3} \right] + \frac{m^3d}{64\beta^2\hbar^3\tau\epsilon^2} \text{Re} \left[ \frac{1}{\gamma_1\gamma_2\gamma_3} \right], \quad (\text{C29})$$

and  $a_3'' = \theta_3'' + \mu_3''$ , where

$$\begin{aligned} \theta_3'' = & -\frac{3d^2}{8\beta^2} - \frac{d^2}{16\beta^4} \text{Im} \left[ \frac{1}{\gamma_1} \right] - \frac{d^2}{16\beta^4} \text{Im} \left[ \frac{1}{\gamma_2} \right] + \frac{d^2}{16\beta^4} \text{Im} \left[ \frac{1}{\gamma_3} \right] + \frac{m^2d^2}{4^4\beta^4\hbar^2\epsilon^2} \text{Im} \left[ \frac{1}{\gamma_1^2\gamma_2} \right] - \frac{m^4d^2}{4^6\beta^4\hbar^4\epsilon^2} \text{Im} \left[ \frac{1}{\gamma_1^2\gamma_2^2\gamma_3} \right] \\ & + \frac{m^2d^2}{2^7\beta^4\hbar^2\epsilon^2} \text{Im} \left[ \frac{1}{\gamma_1\gamma_2\gamma_3} \right] + \frac{md^2}{32\beta^4\hbar\epsilon} \text{Re} \left[ \frac{1}{\gamma_1\gamma_2} + \frac{1}{\gamma_2\gamma_3} \right] + \frac{m^2d^2}{4^4\beta^4\hbar^2\epsilon^2} \text{Im} \left[ \frac{1}{\gamma_2^2\gamma_3} \right] - \frac{m^3d^2}{2^9\beta^4\hbar^3\epsilon^3} \text{Re} \left[ \frac{1}{\gamma_1\gamma_2^2\gamma_3} \right], \end{aligned} \quad (\text{C30})$$

$$\mu_3'' = \frac{1}{2} \arctan \left( \frac{\text{Im}[\gamma_0\gamma_1\gamma_2\gamma_3]}{\text{Re}[\gamma_0\gamma_1\gamma_2\gamma_3]} \right), \quad (\text{C31})$$

where

$$\gamma_0 = \frac{1}{2\sigma_0^2} + \frac{Im}{2\hbar t}, \quad (\text{C32})$$

$$\gamma_1 = \frac{1}{2\beta^2} + \frac{Im}{2\hbar t} + \frac{Im}{2\hbar\epsilon} + \frac{m^2}{4\hbar^2 t^2 \gamma_0}, \quad (\text{C33})$$

$$\gamma_2 = \frac{1}{2\beta^2} + \frac{Im}{\hbar\epsilon} + \frac{m^2}{4\hbar^2 \epsilon^2 \gamma_1}, \quad (\text{C34})$$

$$\gamma_3 = \frac{1}{2\beta^2} + \frac{Im}{2\hbar\epsilon} + \frac{Im}{2\hbar\tau} + \frac{m^2}{4\hbar^2 \epsilon^2 \gamma_2}. \quad (\text{C35})$$

The amplitude is given by

$$A_I = \frac{1}{\sqrt{\sigma_0}\sqrt{\pi}} \left( \frac{m^2}{4\hbar^2 \sqrt{t\epsilon^2\tau} |\gamma_0\gamma_1\gamma_2\gamma_3|} \right). \quad (\text{C36})$$

The wave function  $\psi_{\text{loop-BA}}$  for the propagation going through slit B, then to slit A, can be obtained replacing  $d$  with  $-d$  in Eqs. (C26) and (C29).

- 
- [1] T. Young, *A Course of Lectures on Natural Philosophy and the Mechanical Arts* (printed for J. Johnson, P. C. Yard, W. Savage, B. Bury, London, 1807).
- [2] W. H. Bragg and W. L. Bragg, *Proc. R. Soc. London A* **88**, 428 (1913).
- [3] M. Arndt, O. Nairz, J. Vos-Andreae, C. Keller, G. van der Zouw, and A. Zeilinger, *Nature* **401**, 680 (1999).
- [4] A. Viale, M. Vicari, and N. Zanghì, *Phys. Rev. A* **68**, 063610 (2003).
- [5] Y. Aharonov and D. Bohm, *Phys. Rev.* **115**, 485 (1959).
- [6] R. G. Chambers, *Phys. Rev. Lett.* **5**, 3 (1960).
- [7] A. A. Michelson and E. W. Morley, *Am. J. Sci.* **34**, 333 (1887).
- [8] B. P. Abbott, R. Abbott, T. D. Abernathy, M. R. Acernese, F. Ackley, K. Adams, C. Adams, T. Addesso, P. Adhikari, R. X. Adya *et al.*, *Phys. Rev. Lett.* **116**, 061102 (2016).
- [9] M. Born, *Z. Phys.* **37**, 863 (1926).
- [10] R. P. Feynman and A. R. Hibbs, *Quantum Mechanics and Path Integrals*, 3rd ed (McGraw-Hill, 1965).
- [11] T. Padmanabhan, *Quantum Field Theory: The Why, What and How, Graduate Texts in Physics* (Springer International Publishing, 2016).
- [12] H. Yabuki, *Int. J. Theor. Phys.* **25**, 159 (1986).
- [13] R. D. Sorkin, *Mod. Phys. Lett. A* **9**, 3119 (1994).
- [14] R. Sawant, J. Samuel, A. Sinha, S. Sinha, U. Sinha, *Phys. Rev. Lett.* **113**, 120406 (2014).
- [15] O. S Magaña, I. De Leon, M. Mirhosseini, R. Fickler, A. Safarik, U. Mick, B. McIntyre, P. Banzer, B. Rodenburg, G. Leuchs, R. W. Boyd, *Nat. Commun.* **7**, 13987 (2016).
- [16] U. Sinha, C. Couteau, T. Jennewein, R. Laflamme, G. Weihs, *Science* **329**, 418 (2010).
- [17] A. Sinha, A. H. Vijay, and U. Sinha, *Sci. Rep.* **5**, 10304 (2015).
- [18] H. De Raedt, K. Michielsen, and K. Hess, *Phys. Rev. A* **85**, 012101 (2012).
- [19] G. Rengaraj, U. Prathwiraj, S. N. Sahoo, R. Somashekhar, and U. Sinha, *New J. Phys.* **20**, 063049 (2018).
- [20] J. P. Cotter, C. Brand, C. Knobloch, Y. Lilach, O. Cheshnovsky, and M. Arndt, *Sci. Adv.* **3**, e1602478 (2017).
- [21] A. R. Barnea, O. Cheshnovsky, and U. Even, *Phys. Rev. A* **97**, 023601 (2018).
- [22] I. G. da Paz, C. H. S. Vieira, R. Ducharme, L. A. Cabral, H. Alexander, and M. D. R. Sampaio, *Phys. Rev. A* **93**, 033621 (2016).
- [23] J. G. G. de Oliveira Jr., G. de Souza, I. G. da Paz, and M. Sampaio, *Ann. Phys.* **387**, 222 (2017).
- [24] J. Q. Quach, *Phys. Rev. A* **95**, 042129 (2017).
- [25] C. H. S. Vieira, H. A. S. Costa, G. de Souza, M. Sampaio, and I. G. da Paz, *Mod. Phys. Lett. A* **34**, 1950233 (2019).

- [26] J. B. Araujo, I. G. da Paz, H. A. S. Costa, C. H. S. Vieira, and M. Sampaio, *Phys. Rev. A* **101**, 042103 (2020).
- [27] I. Bialynicki-Birula and Z. Bialynicka-Birula, *J. Opt.* **19**, 125201 (2017).
- [28] J. R. Oppenheimer, *Phys. Rev.* **38**, 725 (1931).
- [29] O. Keller, *Light: The Physics of the Photon, Series in Optics and Optoelectronics*, 1st ed. (CRC Press, April 19, 2016).
- [30] Brian J. Smith and M. G. Raymer, *New J. Phys.* **9**, 414 (2007).
- [31] J. H. Field, *Ann. Phys.* **321**, 627 (2006).
- [32] O. Keller, *Phys. Rev. A* **62**, 022111 (2000).
- [33] P. L. Saldanha and C. H. Monken, *New J. Phys.* **13**, 073015 (2011).
- [34] I. Bialynicki-Birula, *Acta Phys. Pol. A* **86**, 97 (1994); *idem*, *Photon Wave Function*, Progress in Optics XXXVI, edited by E. Wolf Amsterdam (Elsevier, Amsterdam, 1996); J. E. Sipe, *Phys. Rev. A* **52**, 1875 (1995).
- [35] J. Schneeloch, and J. C. Howell, *J. Opt.* **18**, 053501 (2016).
- [36] S. P. Walborn, C. H. Monken, S. Pádua, and P. H. Souto Ribeiro, *Phys. Rep.* **495**, 87 (2010).
- [37] C. Couteau, *Contemp. Phys.* **59**, 291 (2018).
- [38] C. K. Law and J. H. Eberly, *Phys. Rev. Lett.* **92**, 127903 (2004).
- [39] E. J. S. Fonseca, C. H. Monken, and S. Pádua, *Phys. Rev. Lett.* **82**, 2868 (1999); C. H. Monken, P. H. Souto Ribeiro, and S. Pádua, *Phys. Rev. A* **57**, 3123 (1998).
- [40] M. V. Fedorov, Y. M. Mikhailova, and P. A. Volkov, *J. Phys. B: At. Mol. Opt. Phys.* **42**, 175503 (2009).
- [41] A. Paul and T. Qureshi, *Quanta* **7**, 1 (2018).
- [42] A. Bramon and R. Escribano, [arXiv:quant-ph/0507040](https://arxiv.org/abs/quant-ph/0507040).
- [43] J. C. Howell, R. S. Bennink, S. J. Bentley, and R. W. Boyd, *Phys. Rev. Lett.* **92**, 210403 (2004); M. P. Edgar, D. S. Tasca, F. Izdebski, R. E. Warburton, J. Leach, M. Agnew, G. S. Buller, R. W. Boyd, and M. J. Padgett, *Nat. Commun.* **3**, 984 (2012); R. S. Bennink, S. J. Bentley, R. W. Boyd, and J. C. Howell, *Phys. Rev. Lett.* **92**, 033601 (2004); I. Ali Khan, and J. C. Howell, *Phys. Rev. A* **73**, 031801(R) (2006).
- [44] G. Dillon, *Eur. Phys. J. Plus* **127**, 66 (2012).
- [45] G. W. Ford, Y. Gao, and R. F. O'Connell, *Opt. Commun.* **283**, 831 (2010).
- [46] A Ghesquire, and T. Dorlas, *Phys. Lett. A* **377**, 2831 (2013).
- [47] M. Ostermeyer, D. Korn, D. Puhlmann, C. Henkel, and J. Eisert, *J. Mod. Opt.* **56**, 1829 (2009).
- [48] L.-M. Duan, G. Giedke, J. I. Cirac, and P. Zoller, *Phys. Rev. Lett.* **84**, 2722 (2000).
- [49] R. Simon, *Phys. Rev. Lett.* **84**, 2726 (2000).
- [50] J. Jacobson, G. Björk, I. Chuang, and Y. Yamamoto, *Phys. Rev. Lett.* **74**, 4835 (1995).
- [51] J. Schneeloch, S. H. Knarr, D. J. Lum, and J. C. Howell, *Phys. Rev. A* **93**, 012105 (2016).
- [52] Yu. M. Mikhailova, P. A. Volkov, and M. V. Fedorov, *Phys. Rev. A* **78**, 062327 (2008).
- [53] C. K. Hong and T. G. Noh, *J. Opt. Soc. Am. B* **15**, 1192 (1998).
- [54] G. Brida, E. Cagliero, G. Falzetta, M. Genovese, M. Gramegna, and E. Predazzi, *Phys. Rev. A* **68**, 033803 (2003).
- [55] R. Menzel, A. Heuer, D. Puhlmann, K. Dechoum, M. Hillery, M. J. A. Spähn, W. P. Schleich, *J. Mod. Optics.* **60**, 8694 (2013).
- [56] De-Jian Zhang, S. Wu, Hong-Gui Li, Hai-bo Wang, J. Xiong, and K. Wang, *Sci. Rep.* **7**, 17372 (2017).
- [57] Maple (2020). Maplesoft, a division of Waterloo Maple Inc., Waterloo, Ontario.
- [58] S. E. Brunner, L. Gruber, A. Hirtl, K. Suzuki, J. Marton, and D. R. Schaart, *JINST* **11**, P11004 (2016).
- [59] H. Padmanabhan and T. Padmanabhan, *Phys. Rev. D* **84**, 085018 (2011).
- [60] C. J. S. Ferreira, L. S. Marinho, T. B. Brasil, L. A. Cabral, J. G. G. de Oliveira, Jr., M. Sampaio, and I. G. da Paz, *Ann. Phys.* **362**, 473 (2015).